MICROCOPY RESOLUTION TEST CHART

NATIONAL BUREAU OF STANDARDS 1963 A

STARLAB
DEPARTMENT OF ELECTRICAL ENGINEERING / SEL
STANFORD UNIVERSITY • STANFORD, CA 94305

AD-A149 523

PROPAGATION OF ELECTROMAGNETIC FIELDS ALONG THE SEA/SEA-BED INTERFACE

by

A.S. Inan

Final Technical Report E721-2

February 1984

This document has been approved
for public release and sale; its
distribution is unlimited.

85 01 11 072

Reproduction in whole or in part is permitted for any
purpose of the U.S. Government.

The views and conclusions contained in this document
are those of the authors and should not be inter-
preted as necessarily representing the official
policies, either expressed or implied, of the Office
of Naval Research or the U.S. Government.

REPORT DOCUMENTATION PAGE		READ INSTRUCTIONS BEFORE COMPLETING FORM
1. REPORT NUMBER Final Tech. Report No. E721-2	2. GOVT ACCESSION NO. AD A149513	3. RECIPIENT'S CATALOG NUMBER
4. TITLE *(and Subtitle)* Propagation of Electromagnetic Fields Along the Sea/Sea-Bed Interface		5. TYPE OF REPORT & PERIOD COVERED Final 15 August 1979–15 April 1983
		6. PERFORMING ORG. REPORT NUMBER
7. AUTHOR(s) A. S. Inan		8. CONTRACT OR GRANT NUMBER(s) N00014-79-C-0848
9. PERFORMING ORGANIZATION NAME AND ADDRESS Space, Telecommunications and Radioscience Laboratory Stanford University Stanford, CA 94305		10. PROGRAM ELEMENT, PROJECT, TASK AREA & WORK UNIT NUMBERS Task Area NR 089-121
11. CONTROLLING OFFICE NAME AND ADDRESS Office of Naval Research, Code 414 800 N. Quincy Street Arlington, Virginia 22217		12. REPORT DATE February 1984
		13. NUMBER OF PAGES 70
14. MONITORING AGENCY NAME & ADDRESS*(If different from Controlling Office)*		15. SECURITY CLASS. *(of this report)* Unclassified
		15a. DECLASSIFICATION/DOWNGRADING SCHEDULE

16. DISTRIBUTION STATEMENT *(of this Report)*

Approval for public release, distribution unlimited

17. DISTRIBUTION STATEMENT *(of the abstract entered in Block 20, if different from Report)*

18. SUPPLEMENTARY NOTES

19. KEY WORDS *(Continue on reverse side if necessary and identify by block number)*

ULF & ELF Electromagnetic Waves in the Sea
Sea Floor Communication
VMD, HED
Sea Floor Cables

20. ABSTRACT *(Continue on reverse side if necessary and identify by block number)*

The propagation of electromagnetic fields along the sea/sea-bed interface is considered for frequencies in the ULF/ELF range (frequencies less than 3 kHz) and for three different sources (a vertical magnetic dipole, a horizontal electric dipole, and an infinite cable, all located on the interface). The interface is assumed to be a plane boundary separating the two semi-infinite conducting media representing the sea and the material comprising the sea bed; this assumption enables use to be made of field expressions derived previously

for harmonically-varying current sources located at a plane boundary. The field components are calculated numerically and compared with those that would be produced under the same conditions in sea water of infinite extent. It is found that (1) the fields can propagate to longer distances along the sea floor because of the lower sea-bed conductivities, and (2) new field components are produced as a result of the presence of the sea/sea-bed interface. Some of these new components are larger at longer distances than the other field components; they are also more sensitive to the conductivity of the sea bed at low frequencies. The results also indicate that there is an optimal frequency at which the field components have a maximum amplitude at a certain distance from the source; this phenomenon could have applications in short-range communication and geophysical prospecting.

Propagation of Electromagnetic Fields Along the Sea/Sea-Bed Interface

BY

A. S. INAN

Final Technical Report E721-2

February 1984

DTIC COPY INSPECTED

ABSTRACT

The propagation of electromagnetic fields along the sea/sea-bed interface is considered for frequencies in the ULF/ELF range (frequencies less than 3 kHz) and for three different sources (a vertical magnetic dipole, a horizontal electric dipole, and an infinite cable, all located on the interface). The interface is assumed to be a plane boundary separating the two semi-infinite conducting media representing the sea and the material comprising the sea bed; this assumption enables use to be made of field expressions derived previously for harmonically-varying current sources located at a plane boundary. The field components are calculated numerically and compared with those that would be produced under the same conditions in sea water of infinite extent. It is found that (1) the fields can propagate to longer distances along the sea floor because of the lower sea-bed conductivities, and (2) new field components are produced as a result of the presence of the sea/sea-bed interface. Some of these new components are larger at longer distances than the other field components; they are also more sensitive to the conductivity of the sea bed at low frequencies. The results also indicate that there is an optimal frequency at which the field components have a maximum amplitude at a certain distance from the source; this phenomenon could have applications in short-range communication and geophysical prospecting.

ACKNOWLEDGEMENT

TABLE OF CONTENTS

CHAPTER I. INTRODUCTION

Electromagnetic wave propagation in conducting media has been of practical interest since the beginning of the century. Toward the end of the first World War, limited experimental and theoretical work focused on the generation of electromagnetic fields in, on, and above the sea by submerged cables carrying alternating current [Drysdale, 1924; Butterworth, 1924]. This work was motivated by the use of cable-generated electromagnetic fields for navigation [Wright, 1953]. These fields are also of interest because of the possibility that they could be used for communicating with submarines [Moore, 1951, 1967]. Despite the absorption of electromagnetic energy in sea water, electromagnetic signals with frequencies in the ULF/ELF range (freqencies less than 3 kHz) are able to propagate to moderately great depths in the ocean and, as a result, they can provide a means of communication with deeply submerged submarines [Wait, 1972]. Another application of these signals is in geophysical prospecting. A significant amount of research has used electromagnetic techniques to study the structure of the Earth's crust [Burrows, 1963; Wait and Spies, 1972a,b,c]. Propagation of ULF/ELF signals through the earth has also been of considerable interest for mine communication; in the event of a mine disaster, telephone wires and other normal links of communication could be interrupted, but communication with the trapped miners could still be achieved through the Earth [Wait and Spies, 1973].

The first extensive theoretical study of electromagnetic wave propagation between submerged stations in sea water was reported by Moore [1951], and most of the subsequent theoretical work centered on a sea of infinite extent [Wait, 1952a; Kraichman, 1970] or on the propagation effects associated with the sea surface above a very deep sea [Moore, 1951; Wait and Campbell, 1953; Hansen, 1963; Banos, 1966; Fraser-Smith and Bubenik, 1976; Bannister and Dube, 1977]. These sea-surface studies indicated that if the horizontal distance between the source and observer is larger than several skin depths, the energy received may follow an up-over-down mode above the surface [Moore and Blair, 1961]. This result led to the conclusion that near the sea/sea-bed interface, the energy received may follow an analogous down-under-up mode in a weakly conducting sea bed under certain conditions [Bubenik and Fraser-Smith, 1978].

1

Such a mode has been investigated in a somewhat different context by a number of researchers [Wheeler, 1960; Burrows, 1963; Mott and Biggs, 1963; Wait and Spies, 1972a,b c; King and Smith, 1981]. These studies suggested that a waveguide may exist under both the sea and the continents and that it may become a usable communication link if other above-ground communications are disrupted; it would also have much lower noise levels. In an electrically shallow sea, the sea-surface and sea-floor modes may exist simultaneously. Weaver [1967] analyzed the fields of electric dipoles submerged in sea water, and Ramaswamy [1972] considered a submerged horizontal magnetic dipole, both taking a sea that was one skin depth deep. Ramaswamy also computed the field components when both the source and receiver are located at the sea/sea-bed interface as a function of sea water induction number varying from 0 to 3. Numerical data describing the electromagnetic fields produced by a vertical magnetic dipole submerged in a sea of finite depth [Bubenik and Fraser-Smith, 1978; Fraser-Smith and Bubenik, 1979] reveal the effects of a strongly conducting sea bed. Other electromagnetic methods for obtaining sea-bed conductivities have been proposed [Brock-Nannestad, 1965; Bannister, 1968a,b; Coggon and Morrison, 1970]. Bannister [1968a] observed that the conductivity of the sea bed may be determined by measuring only the horizontal component of the magnetic field produced at the sea/sea-bed interface by a long horizontal line source located at the air/sea interface. Coggon and Morrison [1970] considered a vertical magnetic dipole submerged in sea water and analyzed the electromagnetic fields over various ranges of sea-water induction numbers and sea-bed conductivities. A recent active-source electromagnetic sounding experiment on the ocean floor [Young and Cox, 1981] introduced new possibilities for studying the electrical conductivity of the ocean crust.

This work considers an electrically deep sea and calculates the electromagnetic fields produced on the sea floor by three different sources co-located, along with the receiver, on the sea floor, as illustrated in Fig. 1.1. The effects of the sea surface are neglected because attenuation along the paths of propagation to and from the sea surface is large. Both the sea and sea bed are assumed to be isotropic, homogeneous, and time-invariant conducting media separated by a plane interface. Computations are restricted to frequencies in the ULF/ELF range, since it is only signals in these

bands that can propagate to significant distances through the conducting media before becoming severely attenuated. The displacement current terms in both media are neglected, and this assumption is well justified in these frequency ranges. It is assumed that both media are nonmagnetic, with permeabilities equal to the free-space permeability ($\mu_0 = 4\pi \times 10^{-7}$H/m). The conductivity of the sea water is $\sigma_s = 4$ S/m and the conductivity of the sea bed varies.

The three sources considered are the vertical magnetic dipole (VMD), horizontal electric dipole (HED), and infinite cable (IC). It is assumed that all the fields vary with time as exp($i\omega t$). The amplitudes of the field components for the VMD and HED are obtained numerically through the techniques described by Bubenik [1977]. Three of the components are verified by computing the same components, using expressions derived by Wait [1952, 1961]. The field comp⌐   for the IC are calculated from explicit expressions and numerical inte⌐   .⌐n [Wait, 1953; Inan et al., 1982]. Most of the data are presented in dimensionless form by measuring all distances in terms of the skin depth of the sea water δ_s defineu as

$$\delta_s = (2/\omega\mu_0\sigma_s)^{1/2}$$

where ω is the angular frequency related to frequency f by the relation $\omega = 2\pi f$. The sea-bed conductivity is normalized to the sea-water conductivity by $\sigma' = \sigma_f/\sigma_s$. where σ' is the normalized sea-bed conductivity. The skin depth in the sea bed is related to the skin depth in sea water by $\delta_f = \delta_s/\sqrt{\sigma'}$, and the wavelengths in both media are proportional to the skin depths because of the relation

$$\lambda_{(s,f)} = 2\pi\delta_{(s,f)}$$

In conducting media. the field intensities variy with an exponential term $e^{-d/\delta}$ (where d is the distance from the source) representing 55 dB/wavelength attenuation [Hansen, 1963], and it is this attenuation that limits the range of the electromagnetic signal. Figure 1.2 is a logarithmic plot of skin depth, wavelength, and exponential attenuation in sea water as a function of frequency.

The numerical results obtained in this work should be useful in determining an effective sea-bed conductivity in smooth regions of the sea floor. Stretches of
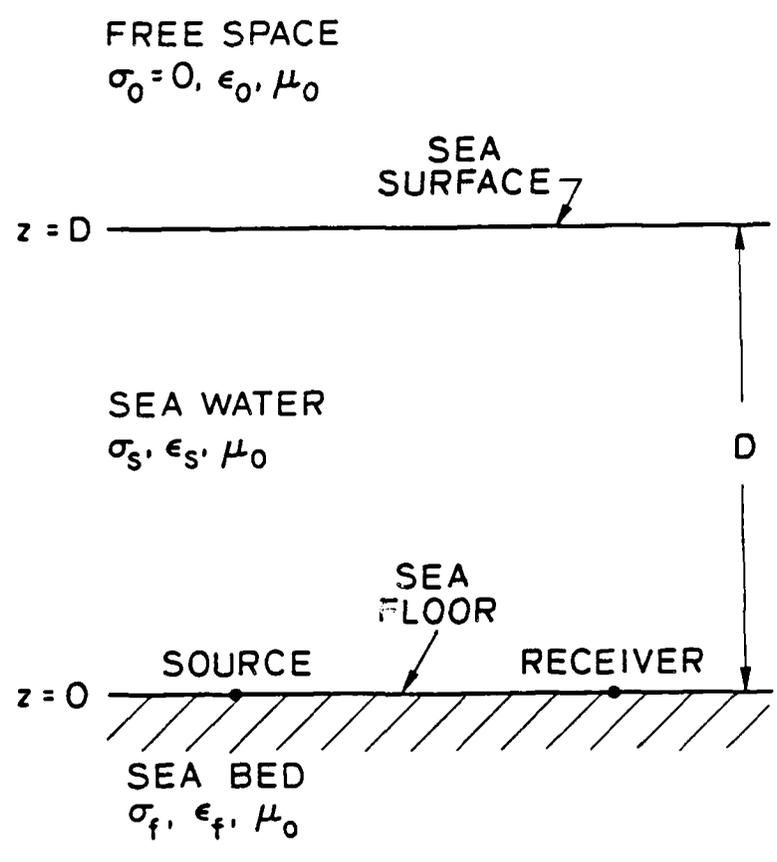
Figure 1.1. Geometry for a source and receiver located on the sea floor.

the abyssal plain in the western North Atlantic have been measured to be smooth within 2 m over distances of 100 km [Pickard and Emery, 1982]. It is also assumed that the sea water shields the sea floor from atmospheric noise and, because the region of interest is far from the shore, the possibility of atmospheric and power-line noise propagating through the Earth's crust can be neglected. This is important because atmospheric noise is especially strong in the ULF/ELF frequency range [Liebermann, 1962; Soderberg, 1969]. The only other possible sources of noise are thermal noise, motions of the sea water (assumed to be negligible), the internal noise of the receiver, and, very speculatively, sources within the Earth's crust.
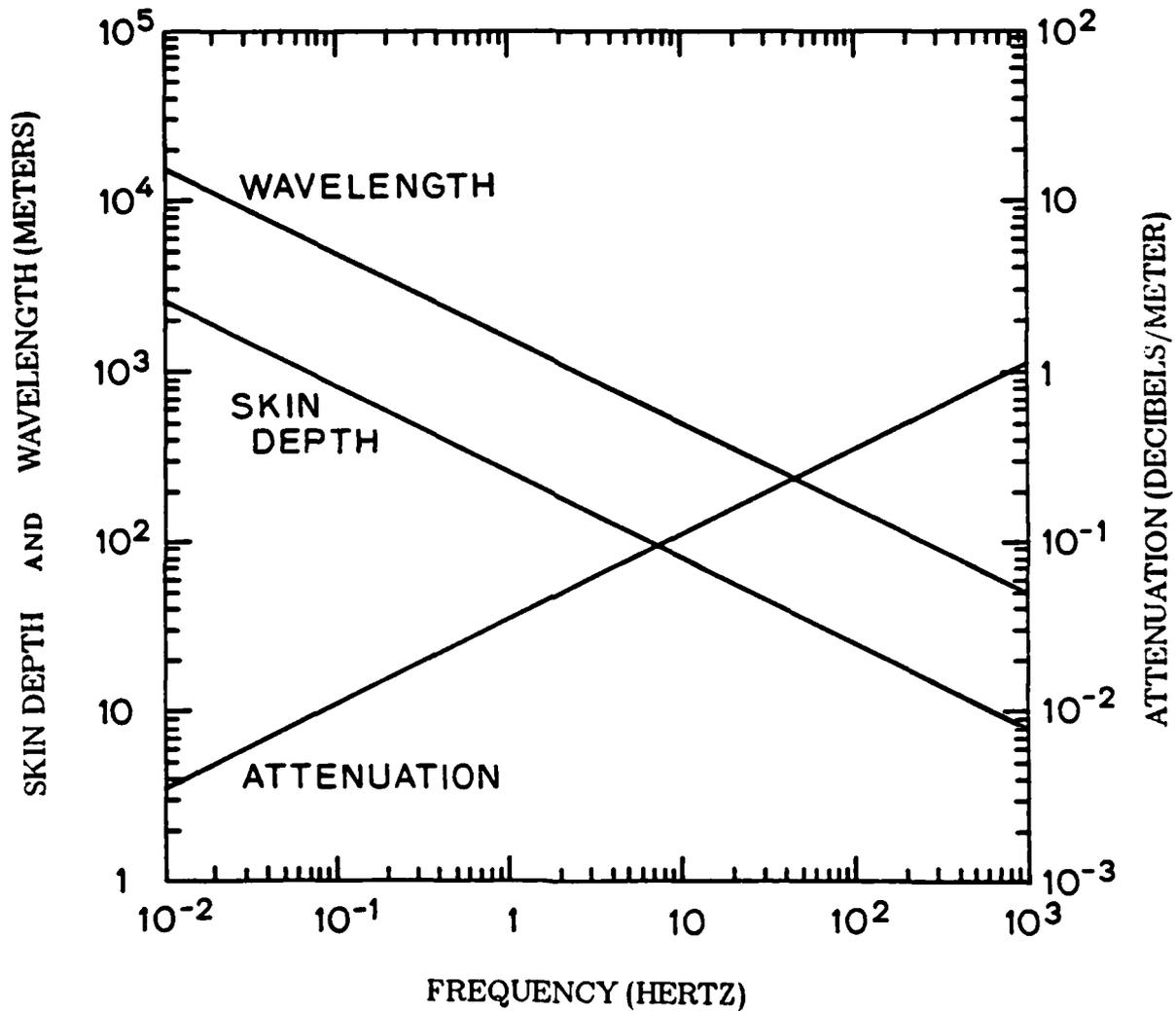
Figure 1.2. Skin depth, wavelength, and exponential attenuation in sea water with a conductivity of 4 S/m (based on Figure A.3 by Kraichman [1976]).

Chapter II. Vertical Magnetic Dipole

In this chapter we consider the electromagnetic fields produced by a small current-carrying insulated wire loop located at the plane interface of two semi-infinite dissipative media. As illustrated in Figure 2.1, the loop is taken to be at the origin of a cylindrical coordinate system (ρ, ϕ, z), with its axis perpendicular to the interface $z=0$ (vertical magnetic dipole). The strength of the magnetic dipole is IdA, where I is the amplitude of the loop current $I\cos\omega t$ and dA is the elementary area of the loop.

A. Derivation of the Field Components

Following Wait [1952] to derive expressions for the field components, the magnetic vector potentials F_e and F_f are first determined for the upper and lower regions, respectively. They have only the following z-components:

$$F_{e,z} = \frac{i\omega\mu_0 IdA}{2\pi} \int_0^\infty \frac{e^{-u_e z}}{u_e + u_f} J_0(\lambda\rho)\lambda \, d\lambda \tag{2.1}$$

$$F_{f,z} = \frac{i\omega\mu_0 IdA}{2\pi} \int_0^\infty \frac{e^{-u_f z}}{u_e + u_f} J_0(\lambda\rho)\lambda \, d\lambda \tag{2.2}$$

where

$$u_e^2 = \lambda^2 + \gamma_e^2, \quad u_f^2 = \lambda^2 + \gamma_f^2$$

$$\gamma_e^2 = i\omega\mu\sigma_e, \quad \gamma_f^2 = i\omega\mu\sigma_f$$

Here, $J_0(\lambda\rho)$ is the Bessel function of the first kind of zero order. The electric and the magnetic fields are related to these potentials by

$$\mathbf{E}_i = -\nabla \times \mathbf{F}_i \tag{2.3}$$

$$\mathbf{B}_i = -\mu_0\sigma_i\mathbf{F}_i + \frac{1}{i\omega}\nabla\nabla\cdot\mathbf{F}_i \tag{2.4}$$

yielding

$$i\omega B_{i,\rho} = \frac{\partial^2 F_{i,z}}{\partial\rho\partial z} \tag{2.5a}$$
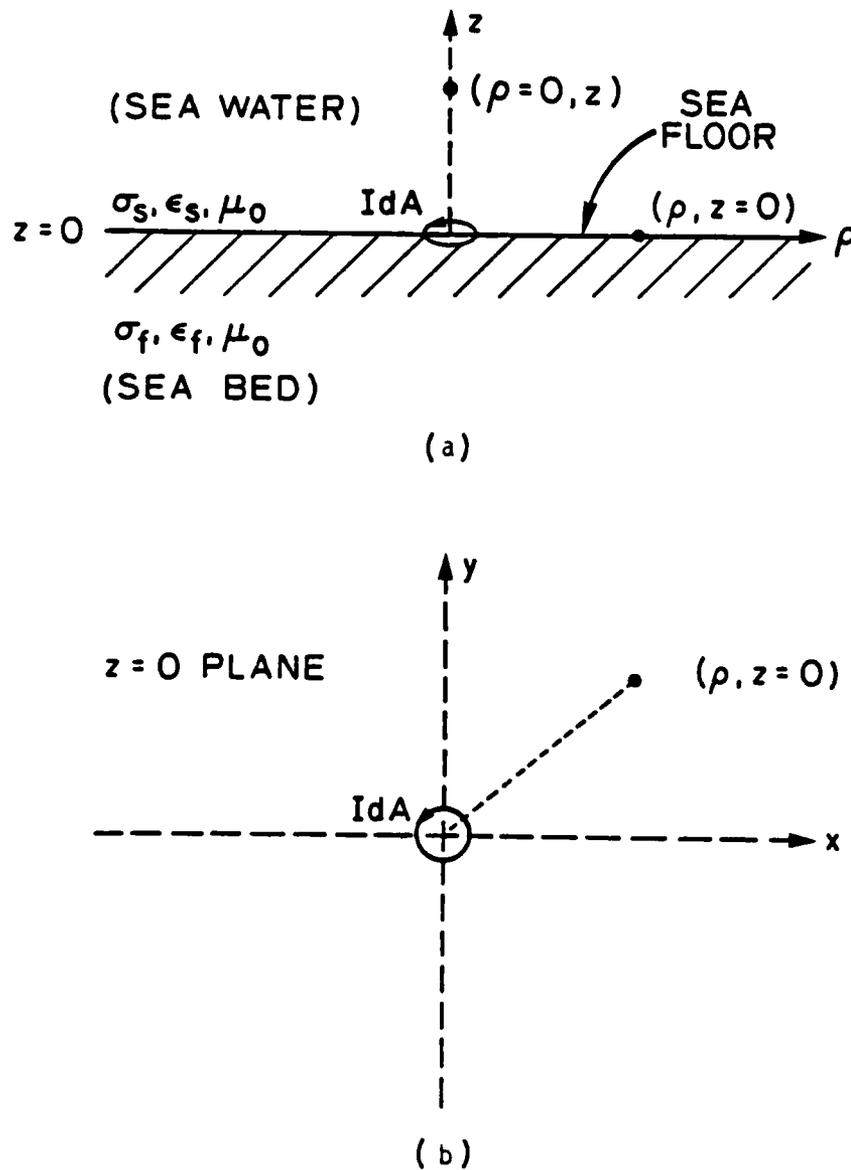
Figure 2.1. Vertical magnetic dipole at the sea/sea-bed interface. (a) Side view, (b) top view, showing azimuthal symmetry.

$$E_{i,\phi} = \frac{\partial F_{i,z}}{\partial \rho} \tag{2.5b}$$

$$i\omega B_{i,z} = -\gamma_i^2 F_{i,z} + \frac{\partial^2 F_{i,z}}{\partial z^2} \tag{2.5c}$$

with $E_{i,\rho} = B_{i,\phi} = E_{i,z} = 0$. The subscript $i = s$ or f depending on whether the fields are in the upper or lower region; therefore,

$$B_{s,\rho} = \frac{\mu_0 I dA}{2\pi} \int_0^\infty \frac{u_s e^{-u_s z}}{u_s + u_f} J_1(\lambda\rho)\lambda^2 \, d\lambda \tag{2.6a}$$

$$E_{s,\phi} = \frac{-i\omega\mu_0 I dA}{2\pi} \int_0^\infty \frac{e^{-u_s z}}{u_s + u_f} J_1(\lambda\rho)\lambda^2 \, d\lambda \tag{2.6b}$$

$$B_{s,z} = \frac{\mu_0 I dA}{2\pi} \int_0^\infty \frac{e^{-u_s z}}{u_s + u_f} J_0(\lambda\rho)\lambda^3 \, d\lambda. \tag{2.6c}$$

When the observation point is on the z-axis ($\rho = 0$), there is only one nonzero field component (the z-component of the magnetic field) along the z-axis,

$$B_{s,z} = \frac{\mu_0 I dA}{2\pi} \int_0^\infty \frac{e^{-u_s z}}{u_s + u_f} \lambda^3 \, d\lambda$$

which can also be expressed as

$$B_{s,z} = \frac{\mu_0 I dA}{2\pi(\gamma_s^2 - \gamma_f^2)} \int_0^\infty (u_s - u_f)e^{-u_s z}\lambda^3 \, d\lambda \tag{2.7}$$

This expression can be rewritten in a dimensionless form by normalizing all distances by the skin depth of the sea water as

$$B_{s,z}^p = \delta_s^3 B_{s,z} = \frac{\mu_0 I dA}{i4\pi(1 - \sigma')} \int_0^\infty (u_s' - u_f')e^{-u_s' z'}\lambda' \, d\lambda' \tag{2.8}$$

where

$$u_s' = \sqrt{\lambda'^2 + i2}, \quad u_f' = \sqrt{\lambda'^2 + i2\sigma'}$$

with $z' = z/\delta_s$, $\lambda' = \delta_s\lambda$, and $\sigma' = \sigma_f/\sigma_s$. Note that, when $\omega = 0$, this magnetic field component becomes

$$B_{s,z} = \frac{\mu_0 I dA}{4\pi z^3}$$

When the observation point is on the plane interface ($z=0$), the field components in Eqs. (2.6) with the exponential term being unity can be expressed in a dimensionless form as

$$B_{e,\rho}^{p} = \delta_e^3 B_{e,\rho} = \frac{\mu_0 IdA}{2\pi} \int_0^\infty \frac{u_e'}{u_e' + u_f'} J_1(\lambda'\rho')\lambda'^2 \, d\lambda' \qquad (2.9a)$$

$$E_{e,\phi}^{p} = \sigma_e \delta_e^4 E_{e,\phi} = \frac{-iIdA}{\pi} \int_0^\infty \frac{1}{u_e' + u_f'} J_1(\lambda'\rho')\lambda'^2 \, d\lambda' \qquad (2.9b)$$

$$B_{e,z}^{p} = \delta_e^3 B_{e,z} = \frac{\mu_0 IdA}{2\pi} \int_0^\infty \frac{1}{u_e' + u_f'} J_0(\lambda'\rho')\lambda'^3 \, d\lambda' \qquad (2.9c)$$

where $\rho' = \rho/\delta_e$. Following Wait[1952], two of the the field components ($E_{e,\phi}$ and $B_{e,z}$), have the following explicit expressions:

$$E_{e,\phi} = \frac{i\omega\mu_0 IdA}{2\pi(\gamma_e^2 - \gamma_f^2)\rho^4}[(3 + 3\gamma_f\rho + \gamma_f^2\rho^2)e^{-\gamma_f\rho} - (3 + 3\gamma_e\rho + \gamma_e^2\rho^2)e^{-\gamma_e\rho}] \quad (2.10)$$

and

$$B_{e,z} = \frac{\mu_0 IdA}{2\pi(\gamma_e^2 - \gamma_f^2)\rho^5}[(9 + 9\gamma_e\rho + 4\gamma_e^2\rho^2 + \gamma_e^3\rho^3)e^{-\gamma_e\rho} \\ -(9 + 9\gamma_f\rho + 4\gamma_f^2\rho^2 + \gamma_f^3\rho^3)e^{-\gamma_f\rho}] \qquad (2.11)$$

The magnetic-field component $B_{e,\rho}$ and the electric-field component $E_{e,\phi}$ are zero at $\omega=0$, and the only nonzero field component $B_{e,z}$ at $\omega=0$ is

$$B_{e,z} = \frac{-\mu_0 IdA}{4\pi\rho^3}$$

B. Numerical Results

The three nonzero field components at the sea/sea-bed interface ($z=0$) are numerically evaluated from the integral expressions in Eqs. (2.6), based on the techniques described by Bubenik [1977]. The dipole moment is set equal to unity (1 Am^2) in these computations; the field amplitudes for any other dipole moment can be obtained quite simply from the computed values by multiplying by the appropriate dipole moment. Note that the electric field unit used in the data presentation is the microvolt/meter and the magnetic field unit is the picotesla.

The amplitudes of the field components are plotted in a dimensionless form for sea-bed conductivities ranging from 1 to 0.001 (1, 0.3, 0.1, 0.03, 0.01, 0.003, and 0.001) times the conductivity of the sea water

Figure 2.2 shows the variations of the magnetic field components B_ρ and B_z, total magnetic field B_T, and total electric field $E_T(= E_\phi)$ as a function of the receiver distance normalized by the skin depth of sea water. As indicated, the fields are all presented in dimensionless form. The results are valid for all frequencies in the range over which the assumptions made in the derivations are valid. The actual field components can be obtained by substituting a numerical value for the skin depth δ_s at the frequency of interest. The observer distance ranges from 0.1 to 100 sea water skin depths. Note that both the vertical and horizontal axes are logarithmic.

The ratios of the field components produced on the sea floor to the field components produced in sea water of infinite extent (*i.e.*, no sea floor) are plotted vs normalized distance in Figure 2.3. The ρ-component of the magnetic field is zero when there is no sea floor present and, as a result, no ratio curves are shown for this component.

It is also possible to plot the field components in another dimensionless form in which the horizontal axis shows the frequency variation for a certain receiver distance. In Figure 2.4, the field components are parametric in terms of the actual distance of the receiver, and the plots reveal the frequency variation of these parametric components. Both axes are drawn with logarithmic scales. Again, the actual field at any receiver distance can be derived from the curves that are shown by substituting the value of the receiver distance.

The results of the numerical integration were verified by calculating two of the field components E_ϕ and B_z, using the explicit expressions in Eqs. (2.10) and (2.11). Some of the low-frequency portions of the curves were also checked by comparing their indicated field values with those obtained from the dc expressions for the field components.

Figure 2.2. Variations in amplitudes of the electric and magnetic fields produced on the sea floor by a vertical magnetic dipole as a function of distance. Note that there are two components of the magnetic field, one parallel and the other perpendicular to the sea/sea-bed interface, and only one component of the electric field parallel to the interface. The dipole moment is unity.
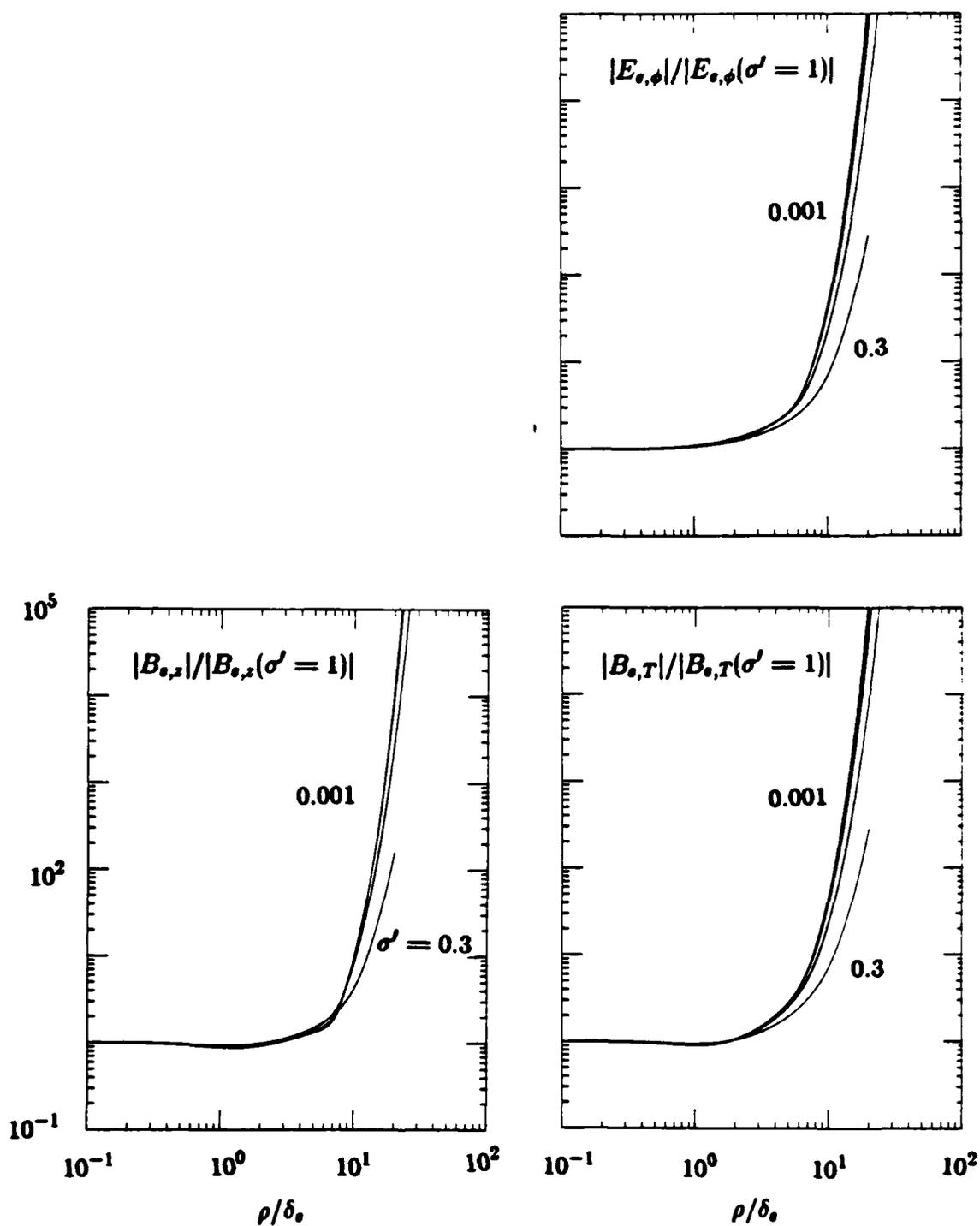
Figure 2.3. Variations in the electric and the magnetic fields produced on the sea floor for an electrically conducting sea bed. The curves show the variation with distance of the ratio of the electromagnetic fields on a sea floor to the fields in an infinitely deep sea water.
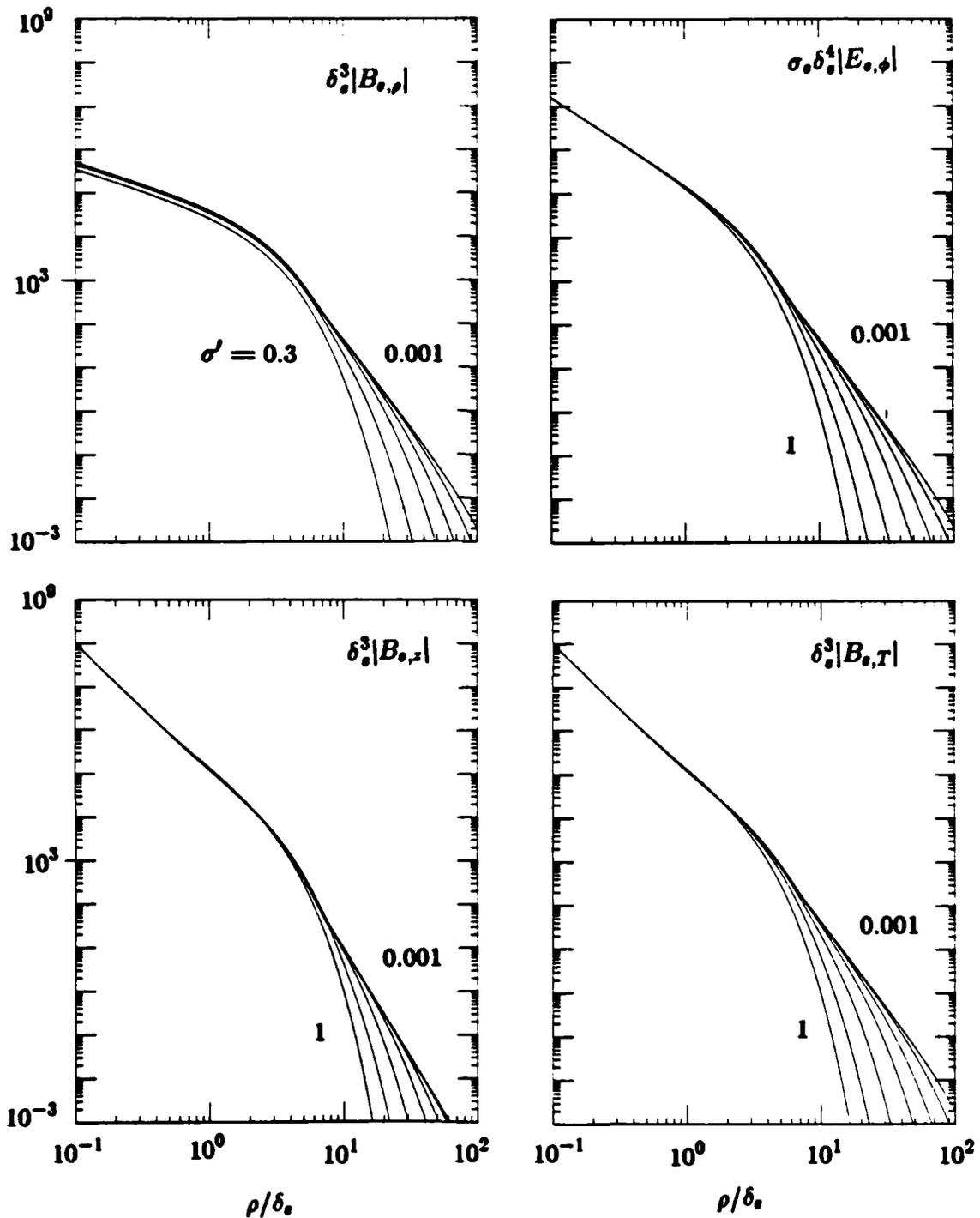
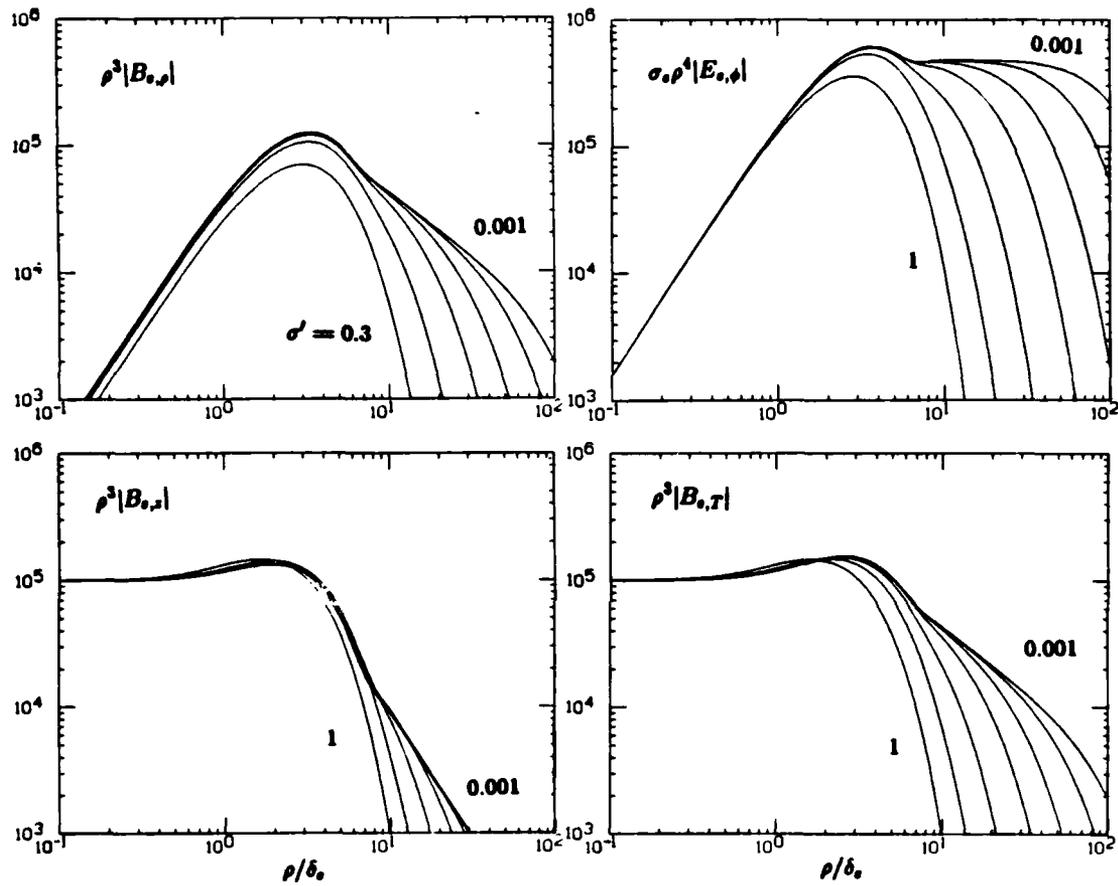Figure 2.4. Variations in the amplitudes of the electric and magnetic fields produced on the sea floor by a vertical magnetic dipole as a function of frequency. The dipole moment is unity.

C. Summary

Based on the numerical results, the presence of the sea floor enables the fields to propagate to longer distances because of the assumed lower conductivity of the sea bed. To take a particular illustrative example, the amplitude of the parametric electric field is $|E_{\theta,\phi}^p| \simeq 1.07$ at a receiver distance of $10\delta_\theta$ on the $z=0$ plane in an infinitely deep sea. On the sea floor, it reaches the same value at a receiver distance greater than $15\delta_\theta$ for a sea-bed conductivity of 0.4 S/m, at a distance greater than $22\delta_\theta$ for 0.04 S/m, and at a distance greater than $25\delta_\theta$ for 0.004 S/m.

A new field component B_ρ is produced as a result of the presence of the sea bed, and it becomes larger than B_z at longer receiver distances. For example, at 100 Hz, and for a sea-bed conductivity of 0.001 times the sea-water conductivity, $|B_{\theta,\rho}| \simeq 6.55 \times 10^{-5}$ pT and $|B_{\theta,z}| \simeq 5.70 \times 10^{-6}$ pT at 632 m. Thus the total magnetic field at 632 m is approximately equal to this new component. The amplitude of the horizontal component of the magnetic field becomes $|B_{\theta,\rho}| \simeq 5.70 \times 10^{-6}$ pT at a receiver distance of 1100 m. This new component is also more sensitive to the conductivity of the sea bed at low frequencies. For example, $|B_{\theta,\rho}^p| = 0.35 \times 10^6$ for $\sigma'=0.3$, 0.45×10^6 for $\sigma'=0.1$, 0.49×10^6 for $\sigma'=0.01$; the other two components are equal to $|E_{\theta,\phi}^p| = 0.16 \times 10^8$ and $|B_{\theta,z}^p| = 0.10 \times 10^9$ for all the above values of σ'.

As can be seen in Figure 2.4, the amplitudes of the fields at a fixed point reach a maximum at a certain optimal frequency. Knowledge of this frequency may be useful for two reasons. First, if the signal is required to be as strong as possible, this frequency should be chosen (assuming that all frequencies are are equally easy to generate). The disadvantage is the limited bandwidth, which restricts the amount of information transmission because the optimal frequency is very low. Second, the effects of the sea floor become significant around this frequency. In Figure 2.4, the curves below the optimal frequency are nearly the same for all sea-bed conductivities; however, above this frequency, they deviate from each other depending on the conductivity of the sea bed.

CHAPTER III. HORIZONTAL ELECTRIC DIPOLE

In this chapter we consider the electromagnetic fields produced by an elementary current source located at the plane interface of two semi-infinite dissipative media. As illustrated in Figure 3.1, the source is assumed to be located at the origin of a cylindrical coordinate system (ρ, ϕ, z), with the plane of separation of the two media corresponding to $z=0$. The source is oriented along the x-axis (*i.e.*, the $\phi=0$ axis) parallel to the interface (horizontal electric dipole) and has an electric-dipole strength of Idl, where I is the amplitude of the sinusoidal source current $I\cos(\omega t)$ and dl is the elementary length of the source.

A. Derivation of the Field Components

For convenience, the Hertz vector components are used instead of the field components. Following Wait [1961], the rectangular components of the Hertz vector in the upper medium are

$$\Pi_{e,x} = C_e \int_0^\infty \frac{e^{-u_e z}}{u_e + u_f} J_0(\lambda\rho)\lambda \, d\lambda \tag{3.1a}$$

$$\Pi_{e,y} = 0 \tag{3.1b}$$

$$\Pi_{e,z} = C_e \cos\phi \int_0^\infty \frac{(u_e - u_f)e^{-u_e z}}{\Delta} J_1(\lambda\rho)\lambda^2 \, d\lambda \tag{3.1c}$$

where

$$C_e = \frac{Idl}{2\pi\sigma_e}, \quad \Delta = \gamma_e^2 u_f + \gamma_f^2 u_e$$

$$\cos\phi = x/\rho, \quad \rho = \sqrt{x^2 + y^2}$$

and the other terms are defined in Chapter II.

The electric and magnetic fields in the upper medium can be obtained using the two vector expressions,

$$\mathbf{E}_e = -\gamma_e^2 \mathbf{\Pi}_e + \boldsymbol{\nabla}\boldsymbol{\nabla}\cdot\mathbf{\Pi}_e \tag{3.2}$$

$$\mathbf{B}_e = \frac{\gamma_e^2}{i\omega}\boldsymbol{\nabla}\times\mathbf{\Pi}_e \tag{3.3}$$
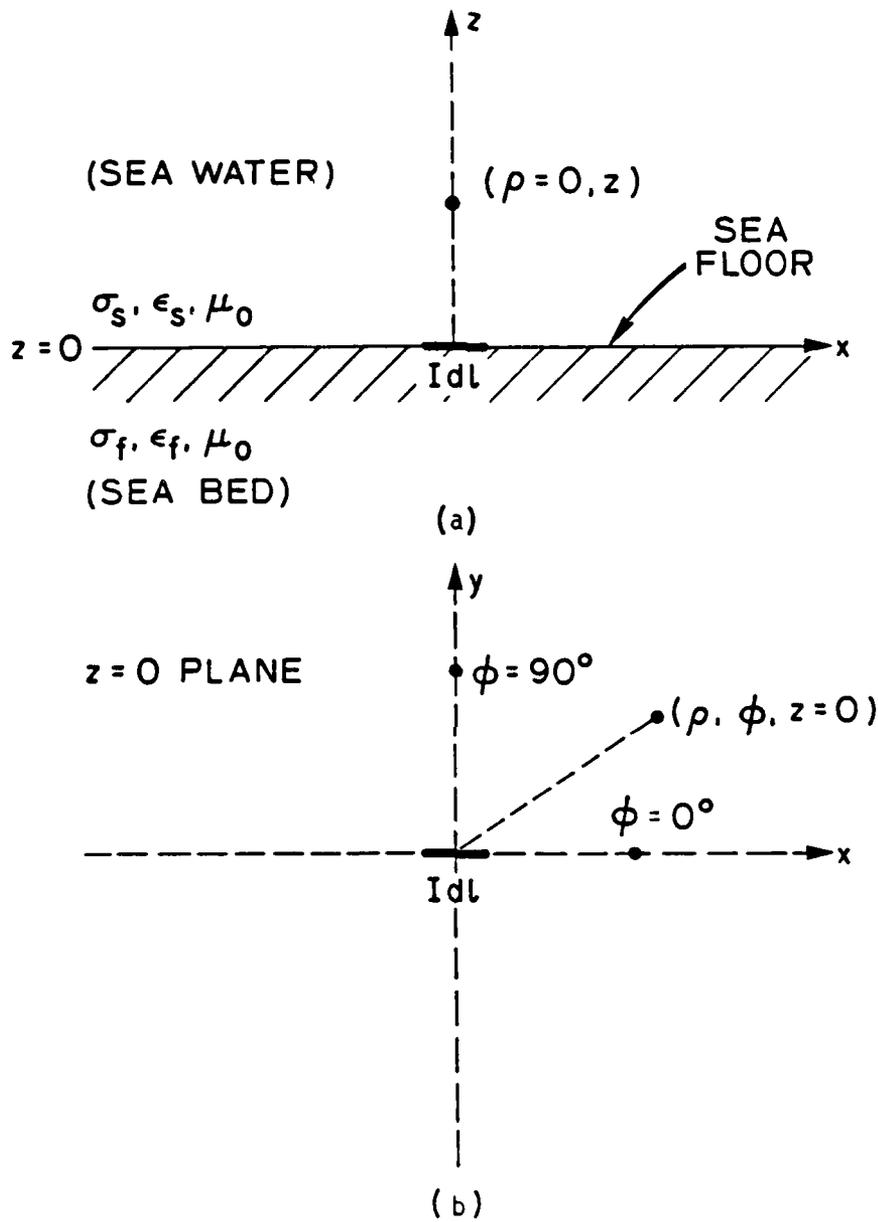
17

Figure 3.1. Horizontal electric dipole located at the sea/sea-bed interface. (a) Side view. (b) top view.

resulting in

$$E_{s,\rho} = -\gamma_s^2 \Pi_{s,\rho} + \frac{\partial(\boldsymbol{\nabla}\cdot\boldsymbol{\Pi}_s)}{\partial \rho} \qquad (3.4a)$$

$$E_{s,\phi} = -\gamma_s^2 \Pi_{s,\phi} + \frac{1}{\rho}\frac{\partial(\boldsymbol{\nabla}\cdot\boldsymbol{\Pi}_s)}{\partial \phi} \qquad (3.4b)$$

$$E_{s,z} = -\gamma_s^2 \Pi_{s,z} + \frac{\partial(\boldsymbol{\nabla}\cdot\boldsymbol{\Pi}_s)}{\partial z} \qquad (3.4c)$$

$$B_{s,\rho} = \frac{\gamma_s^2}{i\omega}\left(\frac{1}{\rho}\frac{\partial \Pi_{s,z}}{\partial \phi} - \frac{\partial \Pi_{s,\phi}}{\partial z}\right) \qquad (3.4d)$$

$$B_{s,\phi} = \frac{\gamma_s^2}{i\omega}\left(\frac{\partial \Pi_{s,\rho}}{\partial z} - \frac{\partial \Pi_{s,z}}{\partial \rho}\right) \qquad (3.4e)$$

$$B_{s,z} = \frac{\gamma_s^2}{i\omega}\left(\frac{1}{\rho}\Pi_{s,\phi} + \frac{\partial \Pi_{s,\phi}}{\partial \rho} - \frac{1}{\rho}\frac{\partial \Pi_{s,\rho}}{\partial \phi}\right) \qquad (3.4f)$$

where $\Pi_{s,\rho}$, $\Pi_{s,\phi}$, and $\Pi_{s,z}$ are the components in the upper medium in cylindrical coordinates. The divergence of the Hertz vector is

$$\boldsymbol{\nabla}\cdot\boldsymbol{\Pi}_s = -C_s\gamma_s^2 \cos\phi \int_0^\infty \frac{e^{-u_s z}}{\Delta} J_1(\lambda\rho)\lambda^2\,d\lambda \qquad (3.5)$$

Based on Eqs. (3.4) the field components can be obtained in the following form:

$$E_{s,\rho} = C_s\gamma_s^2 \cos\phi\left[-\int_0^\infty \frac{u_s u_f e^{-u_s z}}{\Delta} J_0\lambda\,d\lambda + \frac{1}{\rho}\left(\int_0^\infty \frac{u_s u_f e^{-u_s z}}{\Delta} J_1\,d\lambda\right)\right]$$

$$\left[\left(-\int_0^\infty \frac{e^{-u_s z}}{u_s + u_f} J_1\,d\lambda\right)\right] \qquad (3.6a)$$

$$E_{s,\phi} = C_s\gamma_s^2 \sin\phi\left[\int_0^\infty \frac{e^{-u_s z}}{u_s + u_f} J_0\lambda\,d\lambda + \frac{1}{\rho}\left(\int_0^\infty \frac{u_s u_f e^{-u_s z}}{\Delta} J_1\,d\lambda\right)\right]$$

$$\left[\left(-\int_0^\infty \frac{e^{-u_s z}}{u_s + u_f} J_1\,d\lambda\right)\right] \qquad (3.6b)$$

$$E_{s,z} = C_s\gamma_s^2 \cos\phi \int_0^\infty \frac{u_f e^{-u_s z}}{\Delta} J_1\lambda^2\,d\lambda \qquad (3.6c)$$

$$B_{s,\rho} = \frac{C_s \gamma_s^2}{i\omega} \sin\phi \left[-\int_0^\infty \frac{u_s e^{-u_s z}}{u_s + u_f} J_0 \lambda \, d\lambda + \frac{1}{\rho} \left(\int_0^\infty \frac{u_s e^{-u_s z}}{u_s + u_f} J_1 \, d\lambda \right) \right]$$

$$\left[\left(-\gamma_s^2 \int_0^\infty \frac{u_f e^{-u_s z}}{\Delta} J_1 \, d\lambda \right) \right] \tag{3.6d}$$

$$B_{s,\phi} = \frac{-C_s \gamma_s^2}{i\omega} \cos\phi \left[\gamma_s^2 \int_0^\infty \frac{u_f e^{-u_s z}}{\Delta} J_0 \lambda \, d\lambda + \frac{1}{\rho} \left(\int_0^\infty \frac{u_s e^{-u_s z}}{u_s + u_f} J_1 \, d\lambda \right) \right]$$

$$\left[\left(-\gamma_s^2 \int_0^\infty \frac{u_f e^{-u_s z}}{\Delta} J_1 \, d\lambda \right) \right] \tag{3.6e}$$

$$B_{s,z} = \frac{C_s \gamma_s^2}{i\omega} \sin\phi \int_0^\infty \frac{e^{-u_s z}}{u_s + u_f} J_1 \lambda^2 \, d\lambda \tag{3.6f}$$

where the argument of the Bessel functions J_0 and J_1 are the same as Eqs. (3.1). The field components can also be written in a dimensionless form as follows:

$$E^p_{s,(\rho,\phi,z)} = \sigma_s \delta_s^3 E_{s,(\rho,\phi,z)} \tag{3.7a}$$

$$B^p_{s,(\rho,\phi,z)} = \delta_s^2 B_{s,(\rho,\phi,z)} \tag{3.7b}$$

Note that the terms on the left-hand side are independent of receiver distance so that, after the parametric fields are numerically determined, they can be useful for all frequencies in the valid frequency range.

Equations (3.6) can be simplified by considering two observer locations. The first is along the z-axis ($\rho = 0$) where the only nonzero field components are the x-component of the electric field $E_{s,x}$ and the y-component of the magnetic field $B_{s,y}$ given by

$$E_{s,x} = \frac{-C_s \gamma_s^2}{2} \left[\int_0^\infty \frac{u_s u_f e^{-u_s z}}{\Delta} \lambda \, d\lambda + \int_0^\infty \frac{e^{-u_s z}}{u_s + u_f} \lambda \, d\lambda \right] \tag{3.8a}$$

$$B_{s,y} = \frac{-C_s \gamma_s^2}{i2\omega} \left[\gamma_s^2 \int_0^\infty \frac{u_f e^{-u_s z}}{\Delta} \lambda \, d\lambda + \int_0^\infty \frac{u_s e^{-u_s z}}{u_s + u_f} \lambda \, d\lambda \right] \tag{3.8b}$$

which become

$$E_{s,x} = \frac{-Idl}{2\pi(\sigma_s + \sigma_f)z^3} \tag{3.9a}$$

$$B_{s,y} = \frac{-\mu_0 I dl}{4\pi z^2} \qquad (3.9b)$$

The second observer is located at the interface separating the two media ($z{=}0$), where the field components are the same as in Eqs. (3.6) but without $e^{-u_s z}$ in all the integrals. Wait [1961] derived an explicit expression for the z-component of the magnetic field $B_{s,z}$ in the following form:

$$B_{s,z} = \frac{\mu_0 I dl \sin\phi}{2\pi(\gamma_s^2 - \gamma_f^2)\rho^4}[(3 + 3\gamma_f\rho + \gamma_f^2\rho^2)e^{-\gamma_f\rho} - (3 + 3\gamma_s\rho + \gamma_s^2\rho^2)e^{-\gamma_s\rho}] \quad (3.10)$$

Three of these field components $E_{s,z}$, $B_{s,\rho}$, and $B_{s,\phi}$ are zero, for the dc case, and the other three simplify to

$$E_{s,\rho} = \frac{I dl \cos\phi}{\pi(\sigma_s + \sigma_f)\rho^3} \qquad (3.11a)$$

$$E_{s,\phi} = \frac{I dl \sin\phi}{2\pi(\sigma_s + \sigma_f)\rho^3} \qquad (3.11b)$$

$$B_{s,z} = \frac{\mu_0 I dl \sin\phi}{4\pi\rho^2} \qquad (3.11c)$$

B. Numerical Results

The electric and magnetic field components at the sea-floor interface ($z{=}0$) are numerically evaluated from the integral expressions for two azimuthal angles $\phi = 0^0$ and $\phi = 90^0$, using the techniques described by Bubenik [1977]. The field components at any arbitrary ϕ can be obtained from these results by multiplying them by either $\sin\phi$ or $\cos\phi$. The electric dipole moment is set equal to unity (1 Am), and the field components for any arbitrary dipole moment can be determined by multiplying these results by the dipole moment; the units of the electric and magnetic fields are in microvolts/meter and picoteslas. The results are plotted in a dimensionless form for various sea-bed conductivities ranging from 1 to 0.001 (1, 0.3, 0.1, 0.03, 0.01, 0.003, 0.001) multiplied by the sea-water conductivity. The axes are logarithmic.

The amplitudes of the nonzero field components $E_{s,\rho}$, $B_{s,\phi}$, and $E_{s,z}$ and the total electric field $E_{s,T}$ are plotted vs distance in terms of the skin depth of sea

water for an azimuthal angle of $\phi = 0^0$, as illustrated in Figure 3.2. Figure 3.3 plots the variations of the amplitudes of the nonzero field components $B_{s,\rho}$, $E_{s,\phi}$, and $B_{s,z}$ and the total magnetic field $B_{s,T}$ when $\phi = 90^0$. All the results can be converted to the real field values for any frequency by substituting the numerical value of the skin depth δ_s at that frequency and the conductivity σ_s of the sea water. The receiver distance varies from 0.1 to 100 sea water skin depths.

The numerical results for the field components in the alternate dimensionless form can be obtained by holding the distance of the observer constant and varying the frequency, as demonstrated in Figures 3.4 and 3.5, where the increase in the horizontal axis shows the rise in frequency. The actual field values for any arbitrary receiver distance ρ can be calculated from these curves by substituting the numerical value of ρ in the parametric expressions.

The z-component of the magnetic field $B_{s,z}$ was also calculated from the explicit expression in Eq. (3.10), and the results were used to verify those obtained by the numerical integration of $B_{s,z}$. The dc expressions for some of the field components were also used to check the lower frequency portion of the curves.

C. Summary

The ranges of the electromagnetic signals tend to increase as a result of the lower conductivity of the sea bed, as indicated by all the numerical results. For example, when the sea-bed conductivity is 0.01 times the sea-water conductivity, the increase is approximately a factor of 10^5 at distances of 10 to 20 skin depths.

The new field components produced by the existence of the sea floor are the ρ- and ϕ-components of the magnetic field $B_{s,\rho}$ and $B_{s,\phi}$ and the z-component of the electric field $E_{s,z}$. The new magnetic field components $B_{s,\rho}$ and $B_{s,\phi}$ become larger than the z-component of the magnetic field $B_{s,z}$ at longer distances, which results in a greater total magnetic field. The new component of the electric field does not have this property; however, because of its sensitivity to sea-bed conductivity even at low frequencies, it may have useful applications in sea-bed prospecting.

Figures 3.4 and 3.5 show the variations of the fields with frequency. As can be seen, all of the field components are sensitive to the conductivity of the sea bed

Figure 3.2. Variations in the amplitudes of the electric and magnetic fields produced on the sea floor by a horizontal electric dipole at an azimuthal angle of 0^0 as a function of distance. Note that there are two components of the electric field, one parallel and the other perpendicular to the sea floor, and only one component of the magnetic field, directed parallel to the floor. The dipole moment is unity.

Figure 3.3. Variations in the amplitudes of the electric and magnetic fields produced on the sea floor by a horizontal electric dipole at an azimuthal angle of 90^0 as a function of distance. Note that there are two components of the magnetic field, one parallel and the other perpendicular to the sea floor, and only one component of the electric field, directed parallel to the floor. The dipole moment is unity.
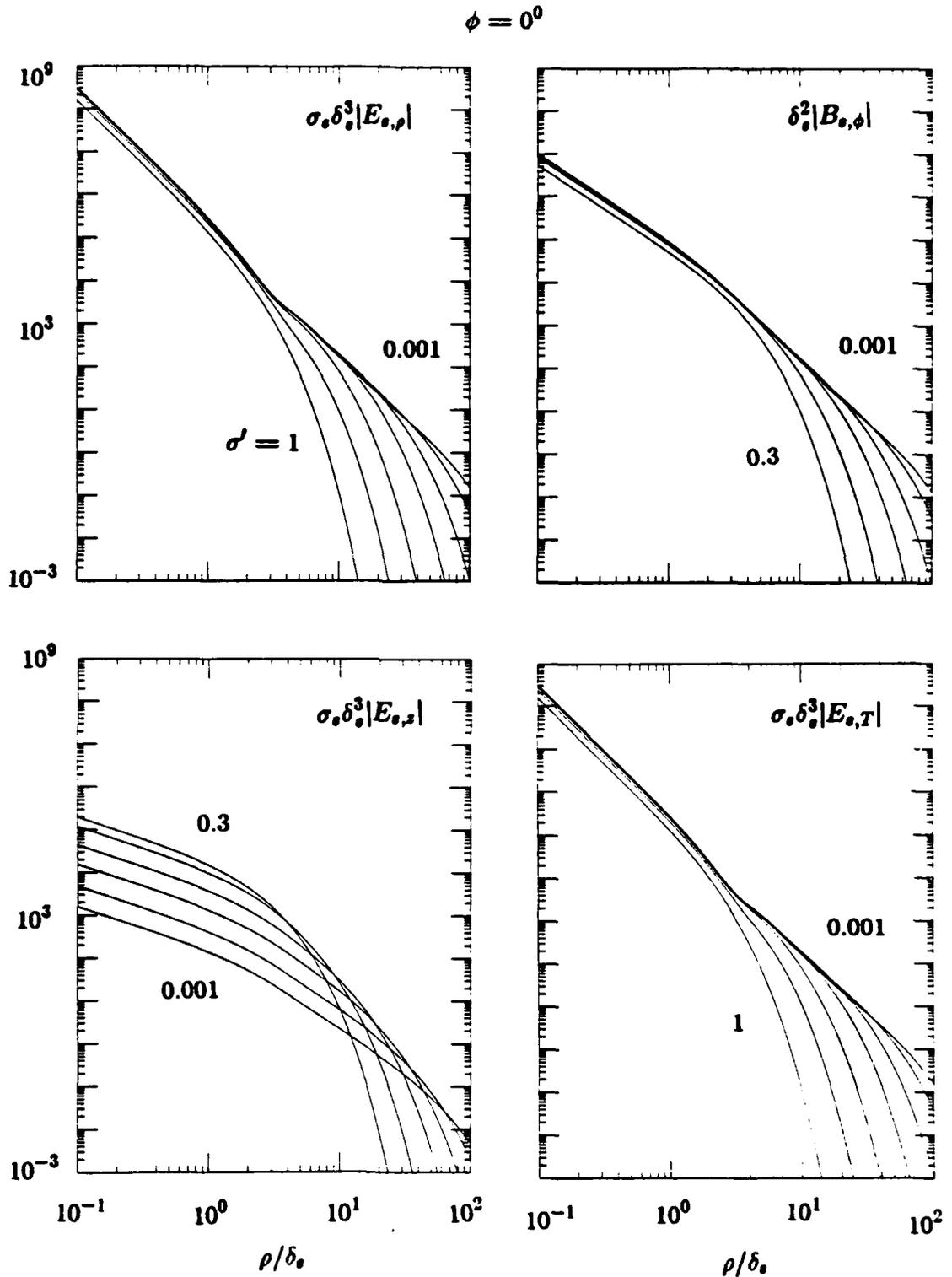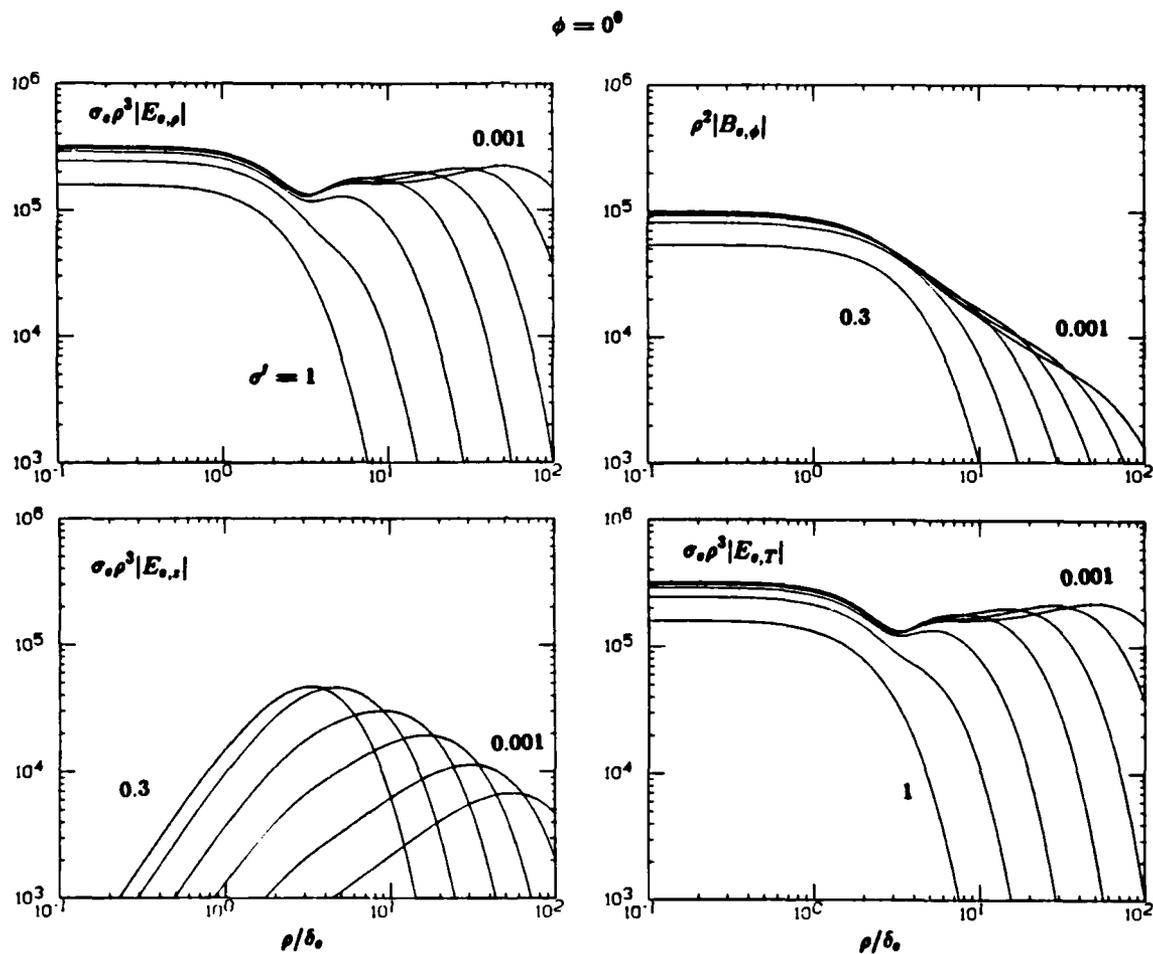
Figure 3.4. Variations in the amplitudes of the electric and magnetic fields produced on the sea floor by a horizontal electric dipole at an azimuthal angle of 0^0 as a function of frequency. The dipole moment is unity.
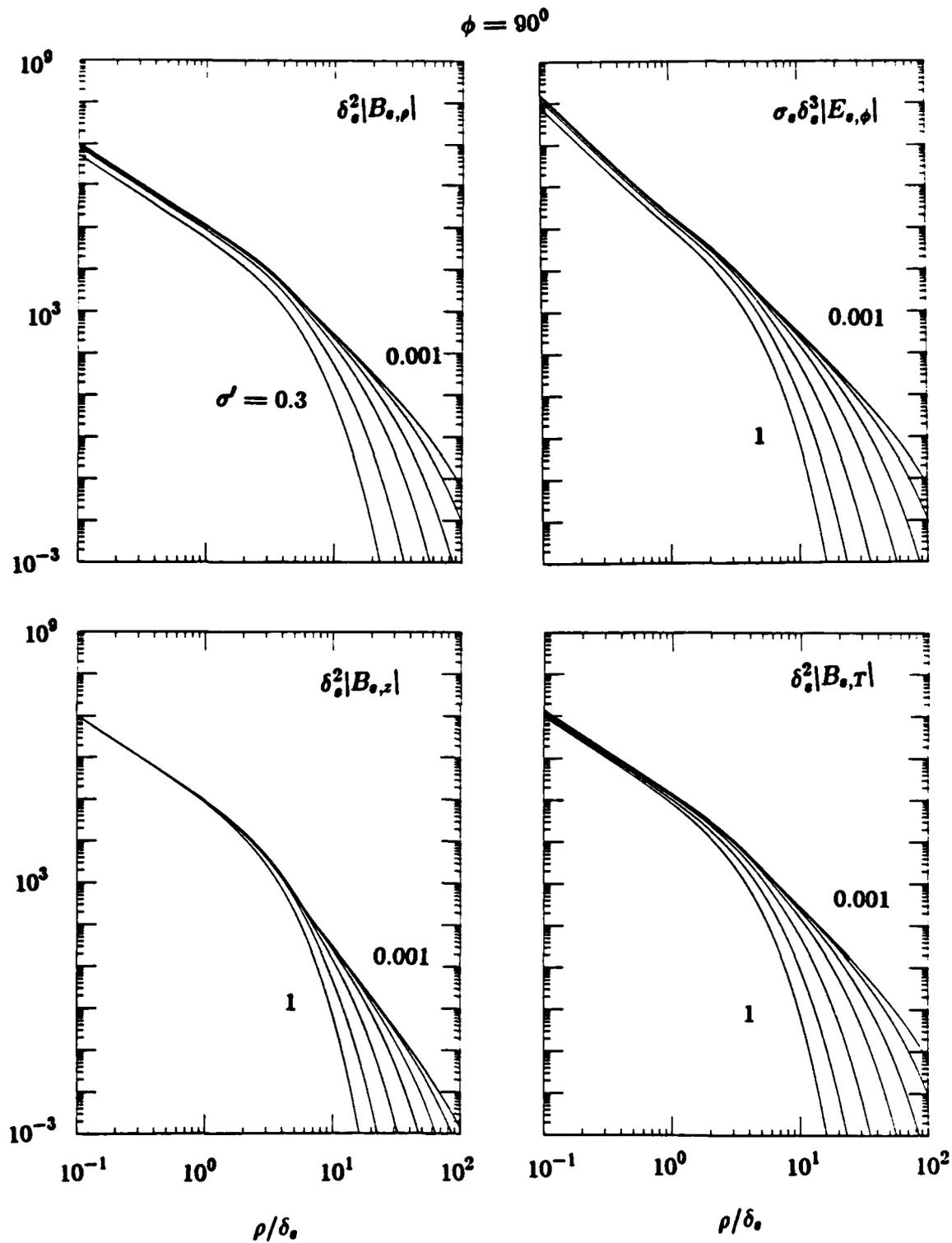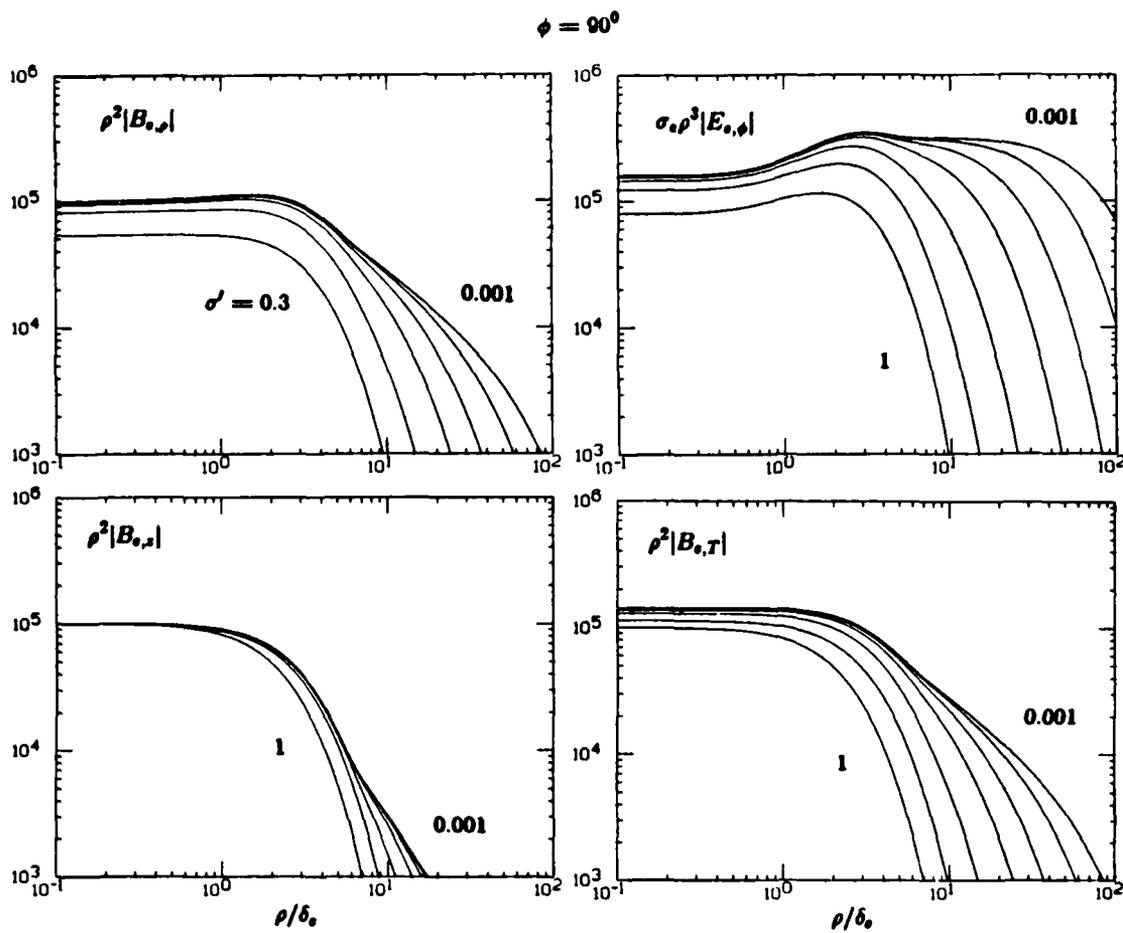
Figure 3.5. Variations in the amplitudes of the electric and magnetic fields produced on the sea floor by a horizontal electric dipole at an azimuthal angle of 90^0 as a function of frequency. The dipole moment is taken to be unity.

at low frequencies except for the vertical component of the magnetic field. The vertical component of the electric field is interesting because it is highly sensitive to sea-bed conductivity at low frequencies and has an optimal frequency that is also sensitive to the same conductivity. Unlike the magnetic field components $B_{s,\rho}$ and $B_{s,\phi}$ produced at the sea floor, this component is not large at long distances and, as a result, it does not contribute to the total electric field.

CHAPTER IV. INFINITE CABLE

In this chapter we consider the electromagnetic fields produced by a straight current-carrying insulated cable of infinite length lying at the plane interface of two conducting media—in our case the interface between the sea and the sea bed. We use the term "infinite" in a relative sense: if the length of the cable is much greater than all the other relevant linear dimensions, it is known as an "infinite" cable. It is assumed to carry an equally distributed alternating current $I \cos \omega t$ at a given instant of time, and this assumption is justified at sufficiently low frequencies [Wait, 1952a; Sunde, 1968]. The cable is oriented along the x-axis, and the plane interface of the two media is $z=0$. Figure 4.1 shows the geometry in the y, z plane; everything is invariant in the x-direction and the direction of the current is taken to be out of the page at $t=0$.

A. Derivation of the Field Components

The Hertz vector components in the upper medium for an HED lying at $z=0$, oriented along the x-axis, and located on the x-axis at $x = l$ are the same as in Eq. (3.1) with x replaced by $x - l$. For an infinite cable, the Hertz vector components can be derived by integrating the components of the Hertz vector for an HED from $l = -\infty$ to $l = \infty$, which results in

$$\Pi_{s,x} = C'_s \int_{-\infty}^{\infty} \int_0^{\infty} \frac{e^{-u_s z}}{u_s + u_f} J_0(\lambda \rho) \lambda \, d\lambda \, dl \tag{4.1a}$$

$$\Pi_{s,y} = 0 \tag{4.1b}$$

$$\Pi_{s,z} = - C'_s \frac{\partial}{\partial x} \int_{-\infty}^{\infty} \int_0^{\infty} \frac{(u_s - u_f)e^{-u_s z}}{\Delta} J_0(\lambda \rho) \lambda \, d\lambda \, dl \tag{4.1c}$$

where

$$C'_s = \frac{I}{2\pi \sigma_s}$$

and all the other quantities were defined in Chapter III. The partial derivative $\partial / \partial x$ can be replaced by $-\partial / \partial l$ to yield
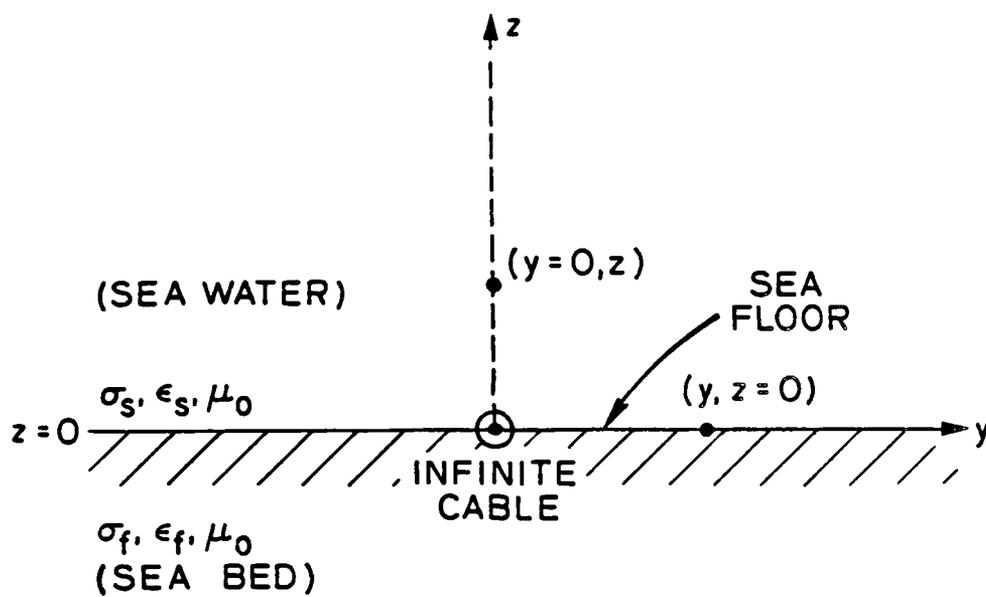
$$\Pi_{s,z} = 0$$

29

Figure 4.1. Infinite cable located at the sea/sea-bed interface. Note the symmetry with respect to the x-axis.

Because the divergence of the Hertz vector is also zero, the only nonzero vector component is the x-component. By using the integral [Sunde, 1968]

$$\int_0^\infty J_0(\lambda\rho)\, dl = \frac{\cos(\lambda y)}{\lambda}$$

the expression for this component can be simplified to

$$\Pi_{e,x} = 2C'_e \int_0^\infty \frac{e^{-u_e z}}{u_e + u_f} \cos(\lambda y)\, d\lambda \qquad (4.2)$$

The electric and magnetic field components can be derived from the Hertz vector via Eqs. (3.2) and (3.3) as

$$E_{e,x} = \frac{-i\omega\mu_0 I}{\pi} \int_0^\infty \frac{e^{-u_e z}}{u_e + u_f} \cos(\lambda y)\, d\lambda \qquad (4.3a)$$

$$B_{e,y} = \frac{-\mu_0 I}{\pi} \int_0^\infty \frac{u_e e^{-u_e z}}{u_e + u_f} \cos(\lambda y)\, d\lambda \qquad (4.3b)$$

$$B_{e,z} = \frac{\mu_0 I}{\pi} \int_0^\infty \frac{\lambda e^{-u_e z}}{u_e + u_f} \sin(\lambda y)\, d\lambda \qquad (4.3c)$$

where $B_{e,x} = E_{e,y} = E_{e,z} = 0$.

As in Chapters II and III, two receiver positions are considered which, to some extent, will simplify the above expressions. When the receiver is located along the line perpendicular to the interface and passes through the infinite cable ($y=0$), $B_{e,z}=0$ and the other two field components become

$$E_{e,x} = \frac{-i\omega\mu_0 I}{\pi} \int_0^\infty \frac{e^{-u_e z}}{u_e + u_f}\, d\lambda \qquad (4.4a)$$

$$B_{e,y} = \frac{-\mu_0 I}{\pi} \int_0^\infty \frac{u_e e^{-u_e z}}{u_e + u_f}\, d\lambda \qquad (4.4b)$$

These expressions can be further simplified by multiplying the numerator and denominator of the integrands by $u_e - u_f$ and following an approach similar to

that used by Wait and Spies [1971]; then,

$$E_{s,x} = \frac{i\omega\mu_0 I}{\pi(\gamma_f^2 - \gamma_s^2)} \left[\frac{\partial^2}{\partial z^2} K_0(\gamma_s z) - \int_0^\infty u_f e^{-u_s z} \, d\lambda \right] \tag{4.5a}$$

$$B_{s,y} = \frac{-\mu_0 I}{\pi(\gamma_f^2 - \gamma_s^2)} \frac{\partial}{\partial z} \left[\frac{\partial^2}{\partial z^2} K_0(\gamma_s z) - \int_0^\infty u_f e^{-u_s z} \, d\lambda \right] \tag{4.5b}$$

Note that $K_0(\gamma_s z)$ is the modified Bessel function of the second kind of zero order and with complex argument. In the dc case, the above two components can be written

$$E_{s,x} = 0, \quad B_{s,y} = -\frac{\mu_0 I}{2\pi z}$$

When the receiver is located at the interface $z=0$, the field components can be written in dimensionless form as

$$E_{s,x}^p = \frac{\pi\sigma_s \delta_s^2}{I} E_{s,x} = -\lim_{z' \to 0} i2 \int_0^\infty \frac{e^{-u_s' z'}}{u_s' + u_f'} \cos(\lambda' y') \, d\lambda' \tag{4.6a}$$

$$B_{s,y}^p = \frac{\sqrt{2}\pi\delta_s}{\mu_0 I} B_{s,y} = -\lim_{z' \to 0} \sqrt{2} \int_0^\infty \frac{u_s' e^{-u_s' z'}}{u_s' + u_f'} \cos(\lambda' y') \, d\lambda' \tag{4.6b}$$

$$B_{s,z}^p = \frac{\sqrt{2}\pi\delta_s}{\mu_0 I} B_{s,z} = \lim_{z' \to 0} \sqrt{2} \int_0^\infty \frac{\lambda' e^{-u_s' z'}}{u_s' + u_f'} \sin(\lambda' y') \, d\lambda' \tag{4.6c}$$

where

$$u_s' = \sqrt{\lambda'^2 + i2}, \quad u_f' = \sqrt{\lambda'^2 + i2\sigma'}$$

and $z' = z/\delta_s$, $y' = y/\delta_s$, $\lambda' = \lambda\delta_s$, and $\sigma' = \sigma_f/\sigma_s$. Wait [1953, 1962] derived explicit expressions for the horizontal electric field component $E_{s,x}$ and the vertical magnetic field component $B_{s,z}$ as

$$E_{s,x} = \frac{i\omega\mu_0 I}{\pi(\gamma_f^2 - \gamma_s^2)y^2} [\gamma_s y K_1(\gamma_s y) - \gamma_f y K_1(\gamma_f y)] \tag{4.7}$$

$$B_{s,z} = \frac{\mu_0 I}{\pi(\gamma_f^2 - \gamma_s^2)y^3}[2\gamma_s y K_1(\gamma_s y) + \gamma_s^2 y^2 K_0(\gamma_s y)$$

$$-2\gamma_f y K_1(\gamma_f y) - \gamma_f^2 y^2 K_0(\gamma_f y)] \tag{4.8}$$

where, again, K_0 and K_1 are the modified Bessel functions of the second kind of order zero and one with complex arguments. The horizontal component of the magnetic field $B_{s,y}$ does not have an explicit expression. When $\omega = 0$, both $E_{s,x}$ and $B_{s,y}$ become zero and the vertical magnetic field component simplifies to

$$B_{s,z} = \frac{\mu_0 I}{2\pi y}$$

B. Numerical Results

This section presents the numerical data for the electric and magnetic field components at the interface of the two conducting media. Two of these components, $E_{s,x}$ and $B_{s,z}$, have explicit expressions [Eqs. (4.7) and (4.8)] that can be expressed in terms of Kelvin functions [Young and Kirk, 1964] and their derivatives. After some algebraic manipulations, their amplitudes can be written in dimensionless form as

$$|E_{s,x}^p| = \frac{\pi \sigma_s \delta_s^2}{I}|E_{s,x}| = \frac{2}{(1 - R^2)\alpha_s}[(c_1 - Rc_2)^2 + (d_1 - Rd_2)^2]^{1/2} \tag{4.9}$$

and

$$|B_{s,z}^p| = \frac{\sqrt{2}\pi\delta_s}{\mu_0 I}|B_{s,z}| = \frac{2}{(1 - R^2)\alpha_s^2}[(\alpha_s(a_1 - R^2 a_2) - 2(d_1 - Rd_2))^2$$

$$+(\alpha_s(b_1 - R^2 b_2) + 2(c_1 - Rc_2))^2]^{1/2} \tag{4.10}$$

where

$$a_1 = ker_0\alpha_s, \quad a_2 = ker_0\alpha_f$$

$$b_1 = kei_0\alpha_s, \quad b_2 = kei_0\alpha_f$$

$$c_1 = ker_0'\alpha_s, \quad c_2 = ker_0'\alpha_f$$

$$d_1 = kei_0'\alpha_s, \quad d_2 = kei_0'\alpha_f$$

and

$$\alpha_s = \sqrt{2}\, y', \quad \alpha_f = R\alpha_s, \quad R^2 = \sigma' = \sigma_f/\sigma_s$$

where α_s and α_f are defined as the induction numbers in the sea water and sea bed respectively [Coggon and Morrison, 1970]. The above expressions for $E_{s,x}$ and $B_{s,x}$ can be evaluated numerically by using tables of Kelvin functions and their derivatives [Lowell, 1959].

The other nonzero component at the interface is the horizontal magnetic field component $B_{s,y}$, and it can be computed only by numerical integration. The expression for it [Eq. (4.6b)] can be divided into two parts,

$$B_{s,y}^p = -\sqrt{2} \int_0^{\lambda'_{max}} \frac{u'_s}{u'_s + u'_f} \cos(\lambda' y')\, d\lambda' - \lim_{z' \to 0} \sqrt{2} \int_{\lambda'_{max}}^{\infty} \frac{u'_s e^{-u'_s z'}}{u'_s + u_{f'}} \cos(\lambda' y')\, d\lambda'$$

Two factors must be determined for numerical integration. The first is λ'_{max}. It is assumed that the effective conductivity of the sea floor is smaller than that of sea water ($\sigma' < 1$). The value for λ'_{max} is chosen such that $\lambda'^2_{max} >> 2$ and, if this constraint is satisfied, both u'_s and u'_f can be approximated as

$$u'_s \simeq \lambda', \quad u'_f \simeq \lambda'$$

for $\lambda' > \lambda'_{max}$. Based on this approximation, the second integral above can be replaced by an explicit term yielding

$$B_{s,y}^p = -\sqrt{2} \int_0^{\lambda'_{max}} \frac{u'_s}{u'_s + u'_f} \cos(\lambda' y')\, d\lambda' + \frac{\sin(\lambda'_{max} y')}{\sqrt{2}\, y'} \tag{4.11}$$

Similarly the integral expression for the vertical component of the magnetic field [Eq. (4.6c)] can be written as

$$B_{s,z}^p = \sqrt{2} \int_0^{\lambda'_{max}} \frac{\lambda'}{u'_s + u'_f} \sin(\lambda' y')\, d\lambda' + \frac{\cos(\lambda'_{max} y')}{\sqrt{2}\, y'} \tag{4.12}$$

The above integrands can be separated into their real and imaginary parts and thus numerically integrated as real integrals. The data for the field components can then be obtained by recombining these terms according to Eqs. (4.11) and (4.12).

The second factor that must be determined is the method of integration. Both integrands are well-behaved functions except for the cosine or sine term that may oscillate rapidly at greater distances than the skin depth of the sea water [Hermance and Peltier, 1970]. Two techniques of numerical integration, Weddle's rule [Computation Laboratory of Harvard University, 1949] and Filon's method [Tranter, 1956], were used. Provided the integration interval is made small enough, both techniques produce sufficiently accurate results.

The computations can be verified in several ways. The first one is to compare the results of the two integration techniques. The second is to compare the results obtained for $B_{e,z}$ through numerical integration using Eq. (4.12) to the results obtained for the same component using Eq. (4.10) and tables of Kelvin functions. The third is to check the lower and higher frequency regions by approximate expressions for these regions.

The left hand panels in Figures 4.2, 4.3, 4.4, and the single panel in Figure 4.5 show the variations in the parametric amplitudes of the three nonzero field components $E_{e,x}^p$, $B_{e,y}^p$, and $B_{e,z}^p$ and the total magnetic field $B_{e,T}^p$ with the induction number of sea water α_e. Note that the parametric terms $\pi \sigma_e \delta_e^2 / I$ and $\sqrt{2}\pi \delta_e / \mu_0 I$ appearing on the left hand side depend on frequency f and not on receiver distance y [see Eqs. (4.6)]. These curves can be used for any frequency in the valid frequency range. The horizontal axis indicates the perpendicular distance of the receiver from the axis of the cable along the sea floor in terms of skin depths of sea water. Each curve corresponds to a different value of R ($R = \sqrt{\sigma_f / \sigma_e}$); R takes the values of 0.01, 0.03, 0.1, 0.3, and 1 except for the $B_{e,y}^p$ component which is zero when $R=1$ (no sea floor). Both axes are plotted on a logarithmic scale, and the units are in volts/meter and teslas.

The right hand panels in Figures 4.2 and 4.4 show the variations of the amplitude ratio of $E_{e,x}$ and $B_{e,z}$ produced on the sea floor to those produced in a sea of infinite depth as a function of distance. The horizontal magnetic field component $B_{e,y}$ is zero in the absence of the sea floor. The second panel in Figure 4.3 plots the variation of the ratio of the amplitude of $B_{e,y}$ to the amplitude of $B_{e,z}$ as a function of distance.
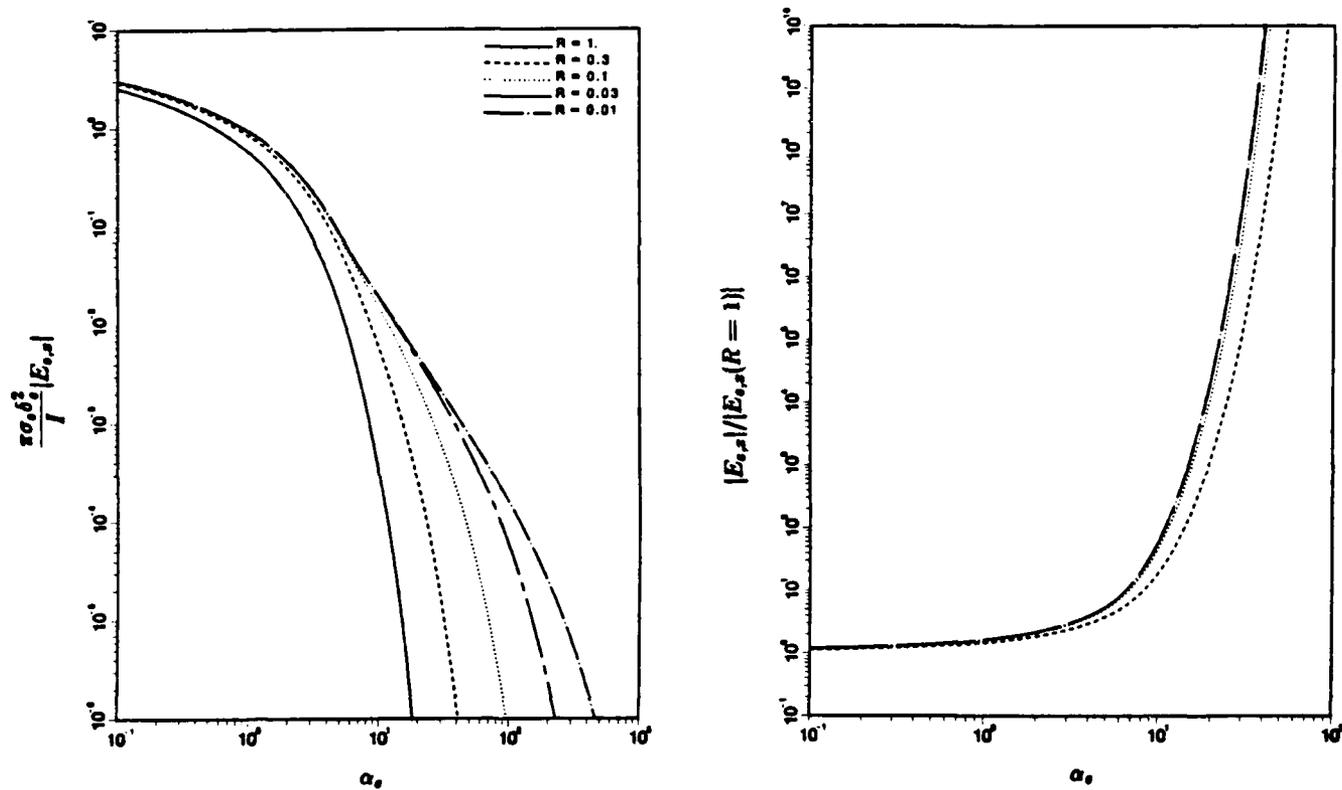
Figure 4.2. Variation with horizontal distance of (1) the amplitude of the electric field produced on the sea floor by an infinite cable (left panel) and (2) of the ratio curves illustrating the changes produced in the electric field by the presence of an electrically conducting sea bed (right). Each curve corresponds to a different sea-bed conductivity. The curves in the right hand panel show the ratio of the electric field at the sea floor to the electric field in an infinitely deep sea.

Figure 4.3. Variation with horizontal distance of (1) the amplitude of the horizontal component of the magnetic field produced on the sea floor by an infinite cable (left panel) and (2) of the ratio of the horizontal component to the vertical component of the magnetic field, both components being measured at the same location on the sea floor (right). Each curve is a function of distance and corresponds to a different sea-bed conductivity.

Figure 4.4. Variation with horizontal distance of (1) the amplitude of the vertical component of the magnetic produced on the sea floor by an infinite cable (left panel) and (2) of the ratio curves illustrating the changes in the vertical component of the magnetic field produced by the presence of an electrically conducting sea bed (right). Each curve corresponds to a different sea-bed conductivity. The curves in the right hand panel show the ratio of the vertical component of the magnetic field produced on the sea floor to the same component in an infinitely deep sea.
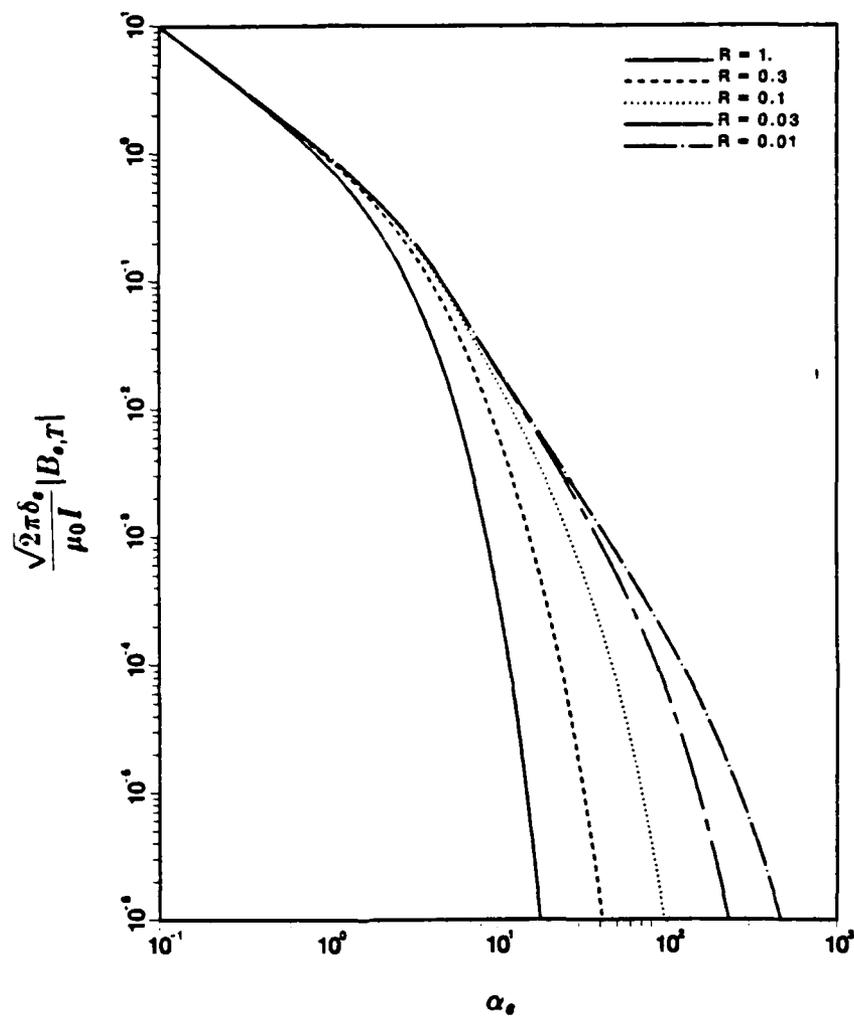
Figure 4.5. Variation with distance of the amplitude of the total magnetic field produced on the sea floor by an infinite cable. Each curve corresponds to a different sea-bed conductivity.
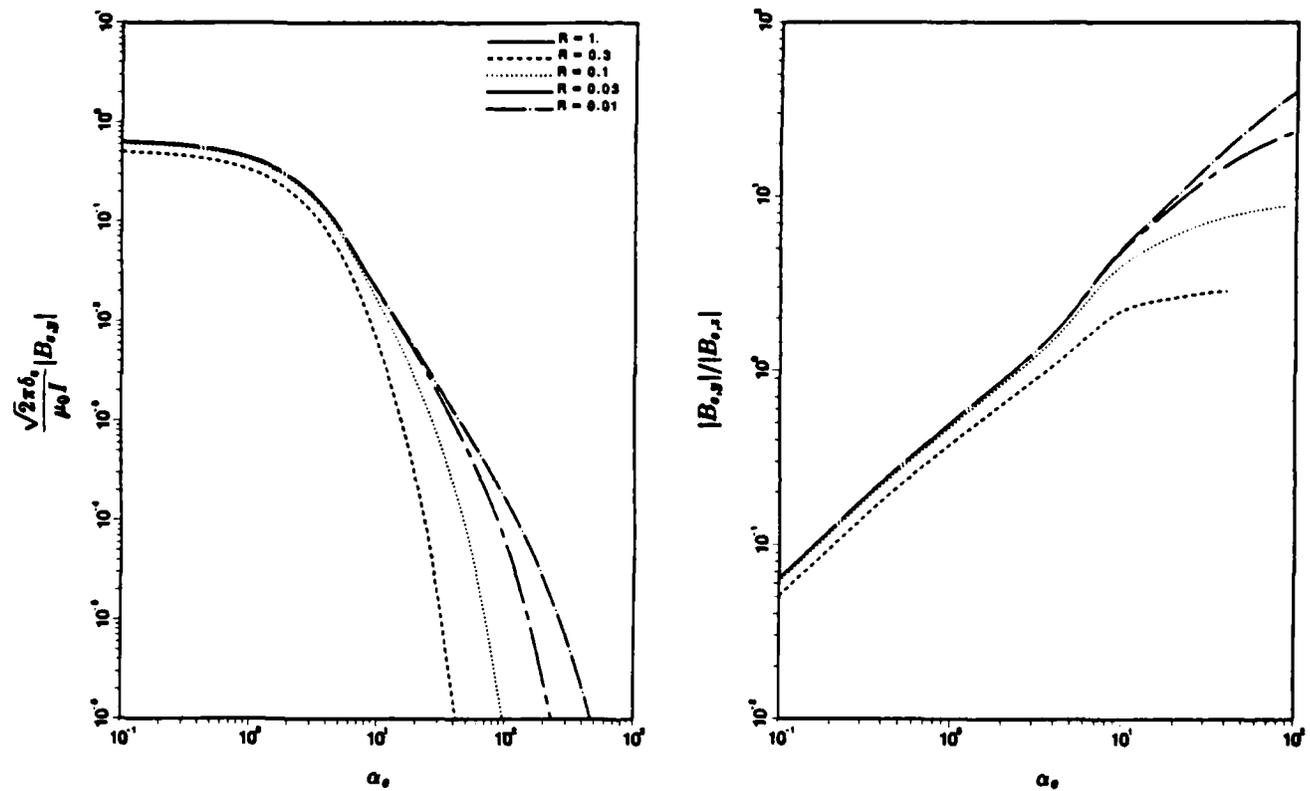
Figure 4.6. Variation with horizontal distance of the amplitudes of the horizontal and vertical components of the magnetic field produced on the sea floor by an infinite cable carrying an alternating current with an amplitude of 1000 A and a frequency of 1 Hz. Each curve corresponds to a different sea-bed conductivity.
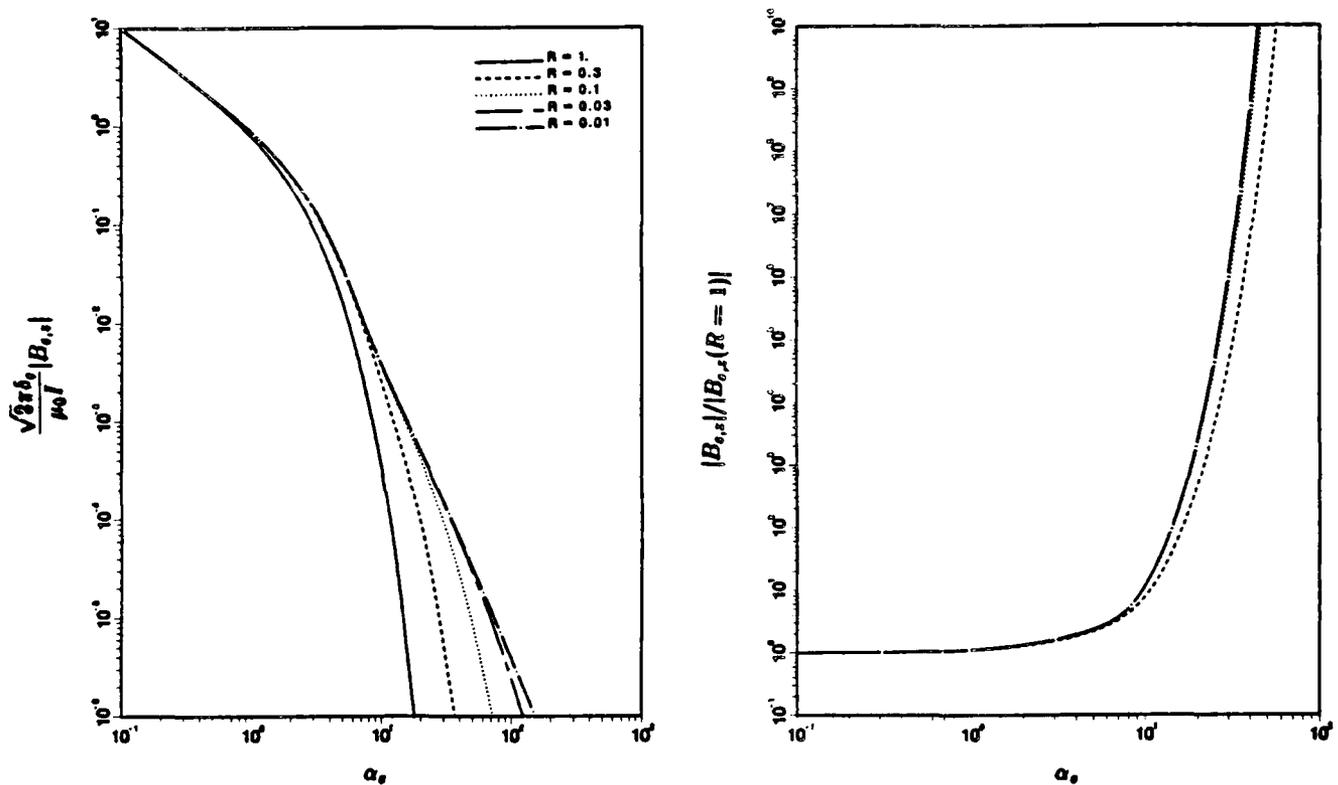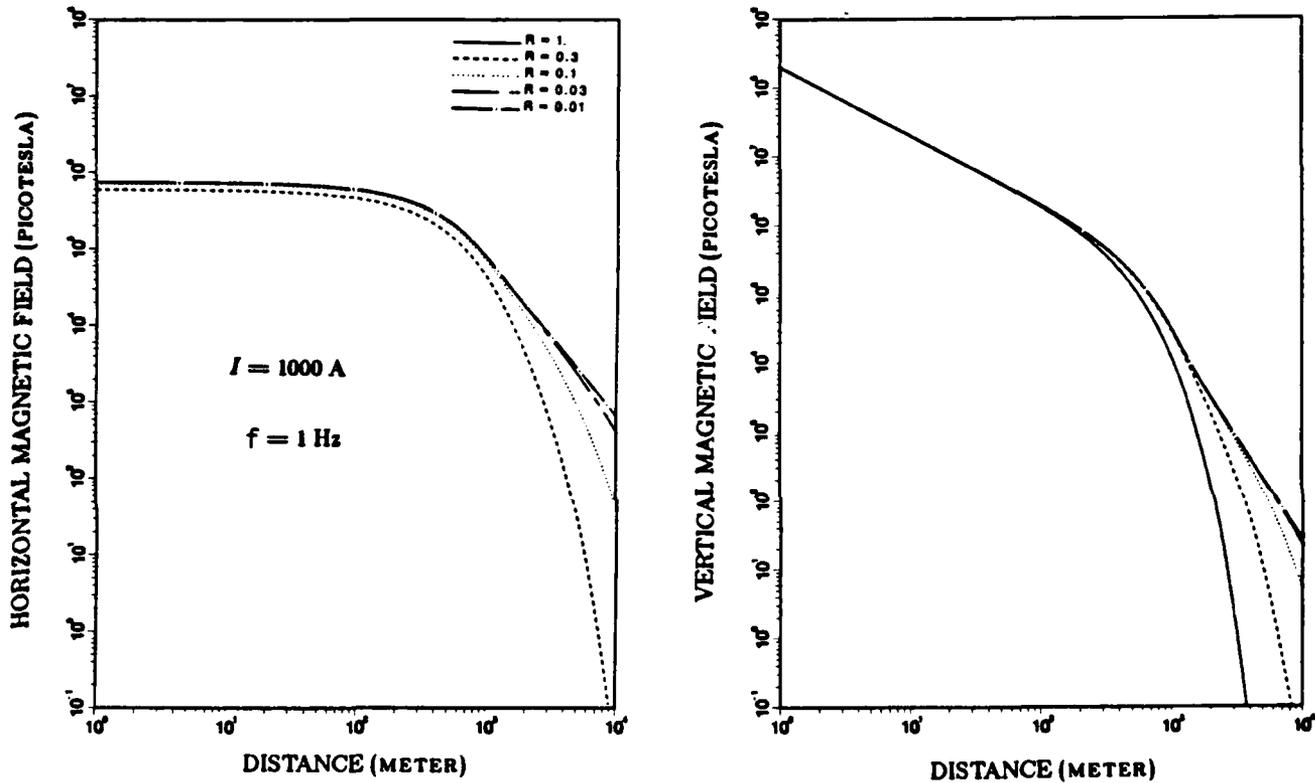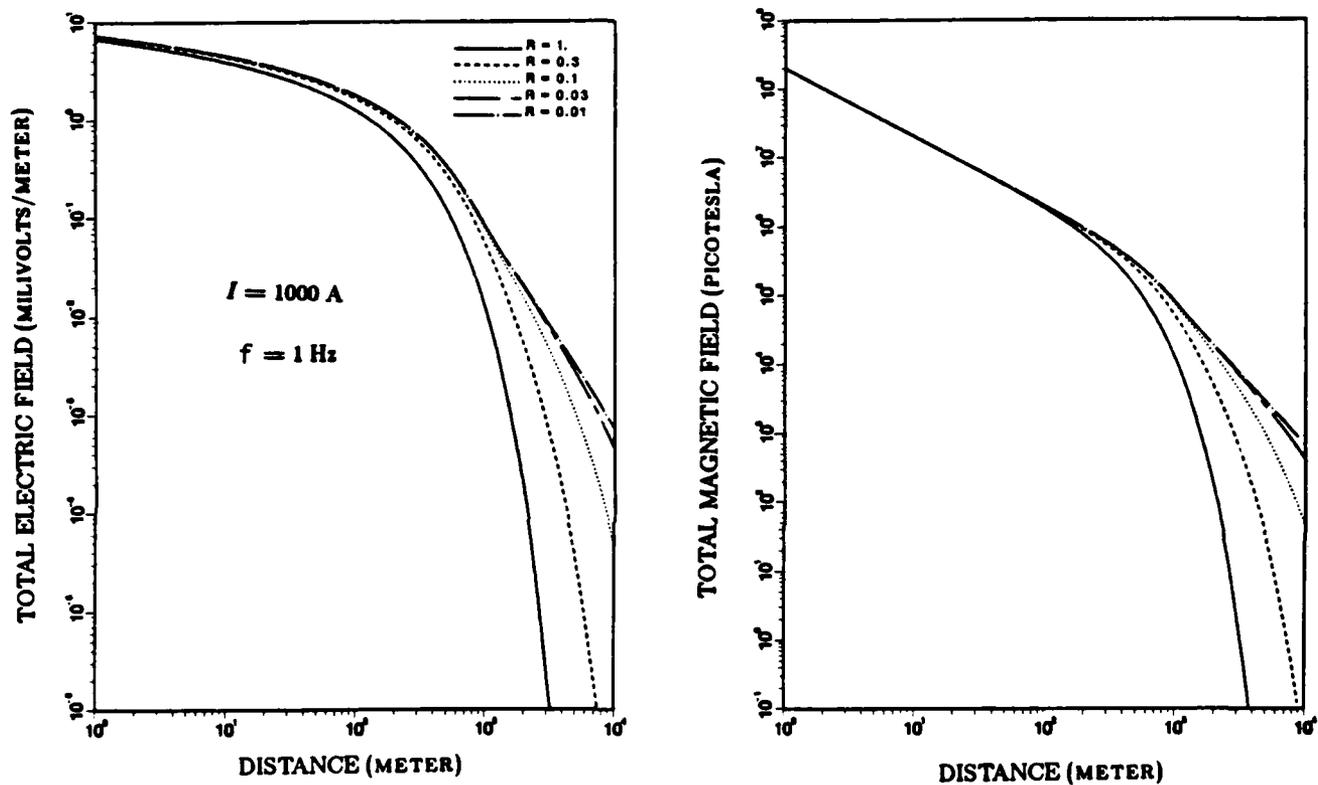
Figure 4.7. Variation with horizontal distance of the amplitudes of the total electric and magnetic fields produced on the sea floor by an infinite cable carrying an alternating current with an amplitude of 1000 A and a frequency of 1 Hz. Each curve corresponds to a different sea-bed conductivity.

In Figures 4.6 and 4.7, the real amplitudes of the field components $E_{s,x}$, $B_{s,y}$, $B_{s,z}$ and the total magnetic field $B_{s,T}$ are plotted vs distance for an alternating current source with an amplitude of 1000 A and a frequency of 1 Hz for the above sea-floor conductivities. The units of electric and magnetic fields are millivolts/meter and picotesla, and distance is in meters.

The above results can be plotted in another parametric form in which the amplitude of the field components is written as

$$|E_{s,x}^p|_y = \frac{2\pi\sigma_s y^2}{I}|E_{s,x}| \tag{4.13a}$$

$$|B_{s,(y,z,T)}^p|_y = \frac{2\pi y}{\mu_0 I}|B_{s,(y,z,T)}| \tag{4.13b}$$

Here, the terms on the left hand side are not functions of frequency but, instead, are functions of receiver distance y. Figures 4.8 and 4.9 plot the variations of the field components in Eqs. (4.13), and the horizontal axis shows the variation in frequency. Note that each curve now corresponds to a different sea-floor conductivity; again, there is no horizontal magnetic field component for $R=1$.

C. Summary

All three field components produced at the interface can propagate farther when a sea floor is present than can those produced in the absence of a sea floor because of the assumed lower conductivity of the sea bed. The increase in range becomes significant at greater distances. For example, when $f=1$ Hz, the amplitude of the horizontal component of the electric field $E_{s,x}$ becomes 1 nV/m at a distance of $y \simeq 3$ km for $\sigma'=1$ (infinitely deep sea), $y \simeq 18$ km for $\sigma'=10^{-2}$, and $y \simeq 90$ km for $\sigma'=10^{-4}$. At 90 km, the source cable must be much longer for it to be an infinite cable; for example, if it is ten times longer (900 km), a uniform current distribution is still a good assumption at 1 Hz [Inan et al., 1983].

The new magnetic field component $B_{s,y}$ is parallel to the interface and perpendicular to the axis of the source. It is negligible when compared to the vertical component $B_{s,z}$ near the cable; however, it becomes comparable to and larger than $B_{s,z}$ at greater receiver distances (Figure 4.3). For example, if $I=1000$ A, $f=1$
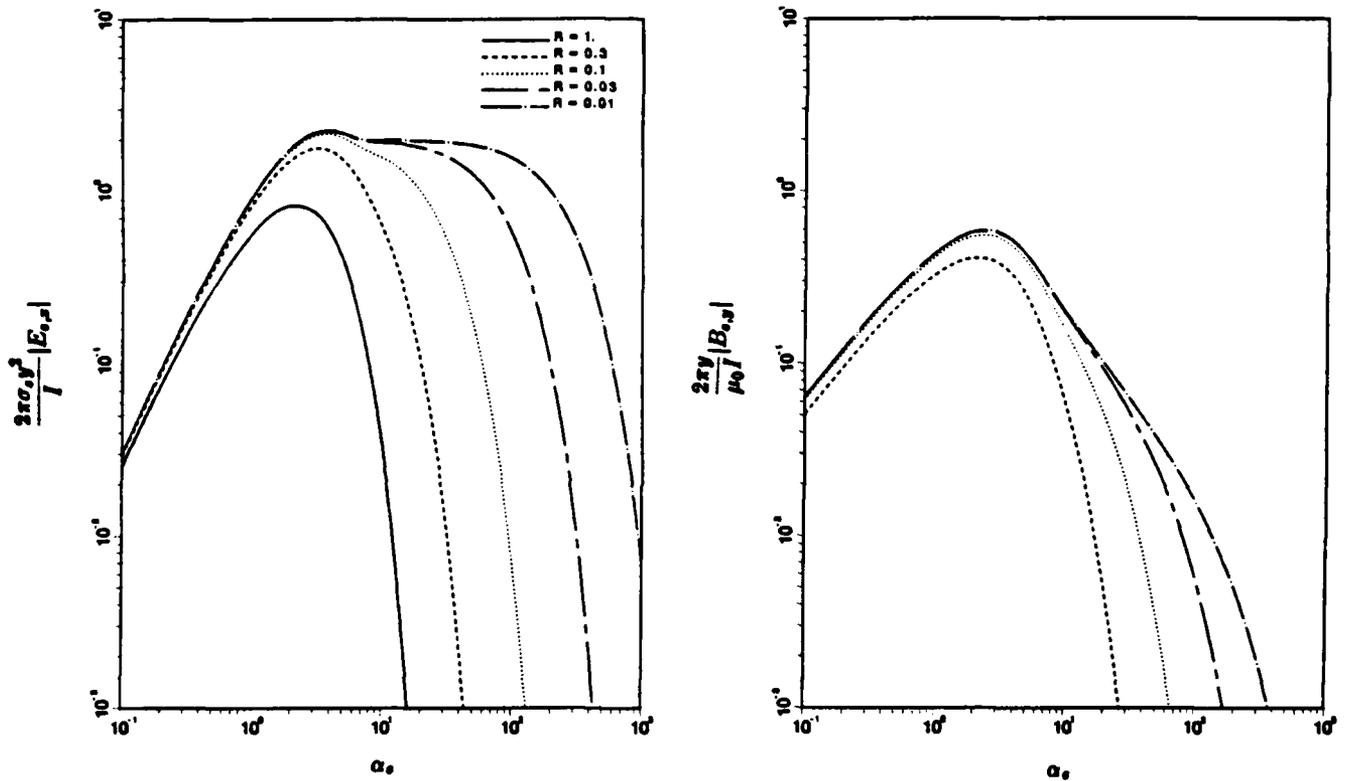
Figure 4.8. Variations in the amplitudes of the total electric field and horizontal component of the magnetic field produced on the sea floor by an infinite cable as a function of frequency. Each curve corresponds to a different sea-bed conductivity.
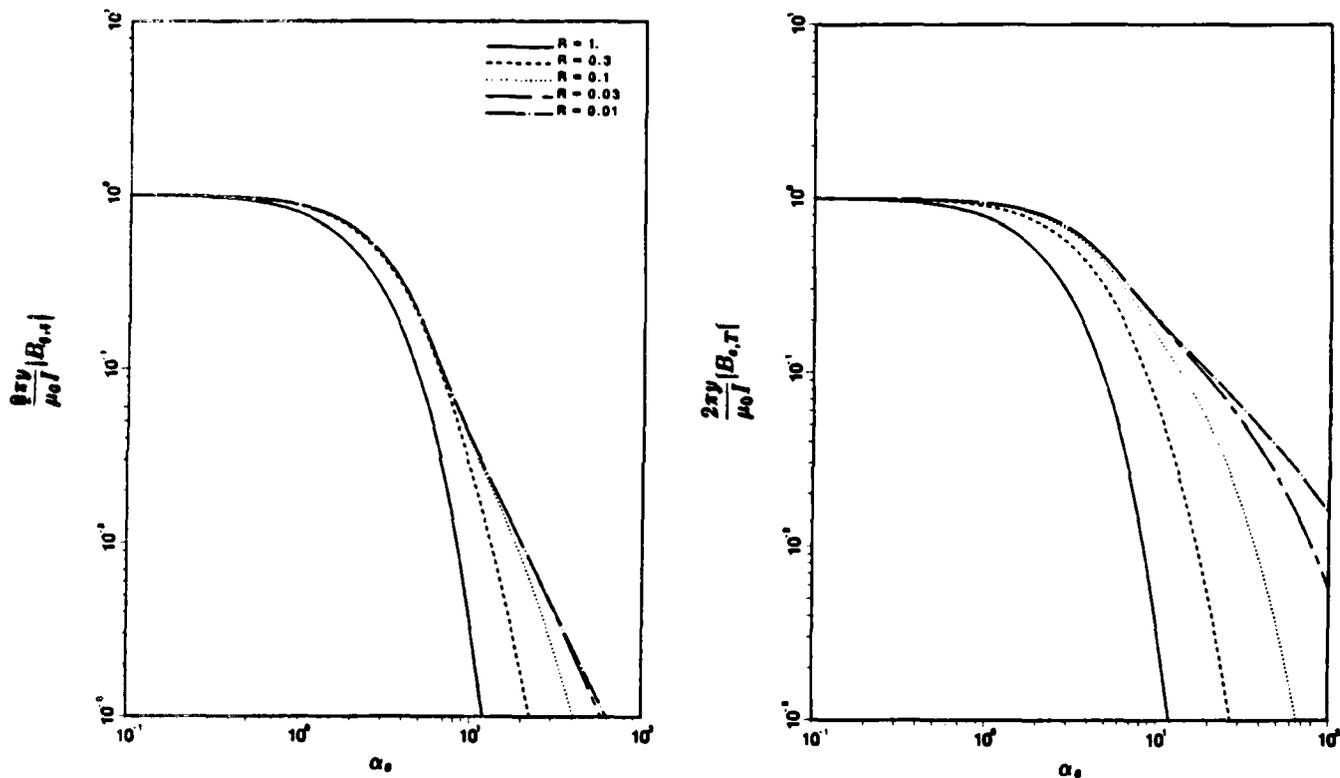
Figure 4.9. Variations in the amplitudes of the vertical component of the magnetic field and the total magnetic field produced on the sea floor by an infinite cable as a function of frequency. Each curve corresponds to a different sea-bed conductivity.

Hz. and $\sigma' = 0.01$, the amplitudes of the horizontal and vertical magnetic field components would be $|B_{s,y}| \simeq 0.70 \times 10^6$ pT and $|B_{s,z}| \simeq 0.20 \times 10^8$ pT at 10 m, 0.57×10^6 and 0.19×10^7 pT at 100 m, and 0.68×10^5 and 0.30×10^5 pT at 1 km. The new component is also more sensitive to the conductivity of the sea bed than are the other two field components at lower frequencies.

The horizontal components of the magnetic and electric fields are zero when $\omega = 0$. They also have optimal frequencies, as observed in Figure 4.8. For example, at a distance of 1 km, the electric field component has an optimal frequency of approximately 0.15 Hz in an infinitely deep sea [Inan et al., 1983].

CHAPTER V. CONCLUSIONS AND RECOMMENDATIONS

A. *Conclusions*

This investigation has concentrated on the electromagnetic fields produced along the sea/sea-bed interface (considered to be a plane boundary between two semi-infinite conducting media) by several different harmonic sources: a vertical magnetic dipole, a horizontal electric dipole, and an infinite cable. New expressions and numerical results have been obtained for the electromagnetic fields produced by these sources. The displacement current terms in both media have been neglected, which is valid for frequencies of less than 100 kHz. The results have been expressed in *two dimensionless forms that make them useful for all frequencies and receiver distances* in the above frequency range. These new results can be summarized as follows.

1) Vertical magnetic dipole: the three nonzero field components at the sea/sea-bed interface are the horizontal magnetic field component in the ρ-direction, the horizontal electric field component in the ϕ-direction, and the vertical magnetic field component in the z-direction. The first is a new component (compared with what would be produced by the same source in a sea of infinite extent under otherwise identical conditions) that can be useful because it (1) becomes larger than the vertical magnetic field component at greater receiver distances, (2) has an optimal frequency at which the amplitude of the field has a maximum, and (3) is more sensitive to the conductivity of the sea bed than the other components at low frequencies. The horizontal electric dipole also has an optimal frequency. Both horizontal components are zero in the dc case and become more sensitive to the conductivity of the sea bed above the optimal frequency than does the vertical component of the magnetic field, which is nonzero in the dc case.

2) Horizontal electric dipole: all six field components are nonzero on the sea floor interface. The two azimuthal angles considered are $\phi = 0^0$ and $\phi = 90^0$. At $\phi = 0^0$, the three nonzero field components are the horizontal component of the electric field along the axis of the source, the horizontal component of the magnetic field perpendicular to the axis of the source, and the vertical component of the electric field perpendicular to the sea floor. Both the horizontal magnetic

field component and the vertical electric field component are the result of the sea/sea-bed interface. The horizontal and especially the vertical component of the electric field are sensitive to the conductivity of the sea bed even at very low frequencies. Another interesting feature is that it has an optimal frequency which, unlike other components, is also very sensitive to the conductivity of the sea bed. At $\phi = 90^0$, the three nonzero field components are the horizontal magnetic field component perpendicular to the axis of the source, the horizontal electric field component parallel to the axis of the source, and the vertical magnetic field component perpendicular to the sea floor. Only the horizontal component of the magnetic field is produced as a result of the sea/sea-bed interface; it becomes larger than the vertical component at greater receiver distances, is sensitive to the conductivity of the sea bed at low frequencies, and is zero at $\omega=0$. The horizontal component of the electric field at $\phi = 90^0$ is also sensitive to the conductivity of the sea bed at low frequencies.

3) Infinite cable: the three nonzero field components at the interface are the horizontal electric field component aligned with the axis of the source, the horizontal magnetic field component perpendicular to the axis of the source, and the vertical magnetic field component perpendicular to the sea floor. The horizontal component of the magnetic field becomes larger than the vertical component at large receiver distances, has an optimal frequency, it is sensitive to the conductivity of the sea bed at low frequencies, and is zero at $\omega=0$. The horizontal component of the electric field is also zero at $\omega=0$ and has an optimal frequency. The vertical component of the magnetic field is nonzero even when $\omega=0$.

The electromagnetic signals produced along the sea floor can propagate farther because of the assumed lower conductivity of the sea bed. Also, new field components are produced as a result of the sea/sea-bed interface and, because they are comparable to and even larger than the components existing in the infinitely deep sea, they produce larger total fields. For example, for an infinite cable carrying alternating current with an amplitude of 1000 A and a frequency of 1 Hz, for a sea-bed conductivity of 1 S/m, the amplitude of the vertical component of the magnetic field is approximately 0.47 pT at a receiver distance of 5 km. The amplitude of the horizontal component of the magnetic field at 5 km is approximately 0.75 pT, which

increases the amplitude of the total magnetic field to roughly 0.88 pT. The new field components are also sensitive to the conductivity of the sea bed; for example, in the case an infinite cable, the parametric amplitude of the horizontal the magnetic dipole is 0.37, 0.50, and 0.61 for $\sigma' = 0.25$, 0.09, and 0.01 at a sea-water induction number of $\alpha_s = 0.1$, whereas the parametric amplitudes of the vertical magnetic dipole at the same sea-bed conductivities and sea-water induction number are 10. Even this component becomes less sensitive to sea-bed conductivity, however, as the conductivity is reduced. The optimal frequency may have some applications for communicating at short ranges and for sea-bed prospecting. For example, for a vertical magnetic dipole, the optimal frequency occurs when the receiver distance is 3 to 4 times the skin depth of sea water and the maximum value of the amplitudes of the horizontal magnetic and electric fields are sensitive to the conductivity of the sea bed at low sea-bed conductivities.

B. Applications

An active experiment has been conducted on the sea floor in the vicinity of the East Pacific Rise to investigate the conductivity of the sea bed by analyzing the measured data [Young and Cox, 1981]. The numerical results that have been obtained in Chapters II, III, and IV could be applied to investigate the effective conductivity of the sea bed (assumed to be homogeneous). Two methods can be used. One is to keep the frequency of the source constant and to vary the observation distance along the interface; however, most of the field components become sensitive to the effective conductivity of the sea bed at distances greater than a skin depth of sea water. The other is to hold the location of the observer constant at the interface and to vary the frequency of the source; in this case the optimal frequency may yield useful information.

Another application is the use of electromagnetic signals for undersea communication. The range of communication with submersibles in the deep parts of the ocean is limited because of the high conductivity of the sea water. The sea bed has an effective conductivity smaller than that of sea water and, as a result, it may provide a new path for the signals along which there will be less attenuation compared to a signal propagating directly through sea water; longer ranges can be

achieved before the signal becomes weak and cannot be detected because of external and internal receiver noise. The sea bed is also a conducting medium and exponential attenuation is still significantly large at high frequencies; therefore, operating frequencies must be low enough to reach long ranges. This limits the bandwidth, and information cannot be transferred at a high data rate.

New field components at the sea/sea-bed interface will increase the ranges of communication. For an infinite cable carrying an alternating current of 1000 A at 1 Hz, and assuming the minimum measurable magnetic field to be 0.1 pT, the field on the sea floor can be detected over a range of approximately 4 km before its amplitude drops below 0.1 pT. The amplitudes of the new horizontal component and the vertical component of the magnetic field along the interface are 0.24 and 0.09 pT at a receiver distance of 8 km for an effective sea bed-conductivity of 0.4 S/m, thus producing a total magnetic field of 0.26 pT. If the sea-bed conductivity is 0.04 S/m, then the two field components are 0.27 and 0.03 pT at a receiver distance of 20 km, and the total magnetic field becomes 0.27 pT as a result of this new component. These two components are about 0.39×10^3 and 0.22×10^2 pT at 20 km for a sea-bed conductivity of 0.004 S/m. These examples indicate that the range of electromagnetic fields along the sea floor increases significantly before their amplitudes drop below the minimum measurable field value.

Arrays of long cables located on the sea floor can achieve longer communication ranges [Inan et al., 1982]. The phases of the currents in each cable can be adjusted to produce a maximum field amplitude at the receiver, which makes communication possible over a much larger area. The separation distance of the cables depends on the amplitudes of the current, frequency, conductivity of the sea bed, sensitivity of the receiver, and background noise. With a series array of cables, each carrying an alternating current of amplitude 1000 A and frequency 1 Hz and separated from each other by 30 skin depths, the magnetic field produced at a point midway between the two cables would be approximately $4 \times 10^2/\delta_s$ or 1.6 pT in an infinitely deep sea; on a sea bed with $\sigma_f = 0.04$ S/m this field would be 4.6×10^3 pT, which indicates that the cables could be moved apart from a spacing of $30\delta_s$ to $140\delta_s$ while still yielding the same field at the center point. Large amounts of power will be lost due to resistive heating in both cases, however, as the source current flows in both

the long cables and surrounding conducting media. The advantage of this system is a less noisy environment in which the electromagnetic signals propagate, since there is significant shielding of atmospheric noise by the large bulk of sea water [Mott and Biggs, 1963].

C. Recommendations

Throughout this investigation, it has been assumed that the sea bed is a homogeneous medium; however, it actually contains layers of sediment with different properties. This work could be extended to two or more layers. For example, in the two-layer bed in Figure 5.1, the first layer has a conductivity of σ_{f1} and extends from $z=0$ to $z=-h$ and the second has a conductivity of σ_{f2} and extends from $z=-h$ to $z=-\infty$. Both the source and receiver are located at the sea/sea-bed interface. The conductivity of the upper layer is larger than that of the lower layer. For receiver distances smaller than the depth of the first layer, the effects of the low-conductivity layer should not be very significant. As receiver distances become larger than the depth of the first layer, however, the signal that follows the down-under-up mode will be much stronger than the signal that directly propagates from the source to the receiver using the sea/sea-bed boundary, and the lower layer will be important. This means that, depending on the location of the observer, the signal at the receiver will carry information about the properties of different layers of the sea bed.

The length of the straight current-carrying cable source was assumed to be infinite. This is a good assumption for a receiver located in the vicinity of the cable (*i.e.*, the perpendicular distance to the receiver is much smaller than the length of the cable) and not close to the ends of the cable. A uniform current distribution along the cable was also assumed. Although this is not true in an infinite cable, the fields produced at the receiver will be the result of the middle portion of the cable because the contribution from the portions toward the ends (not necessarily carrying the same current) will be negligible. As the receiver distance increases, however, a longer portion of the cable must be considered and the uniform-current assumption may no longer be valid. One extension of this work would be to calculate the fields produced on the sea floor by a straight current-carrying insulated cable of finite length.
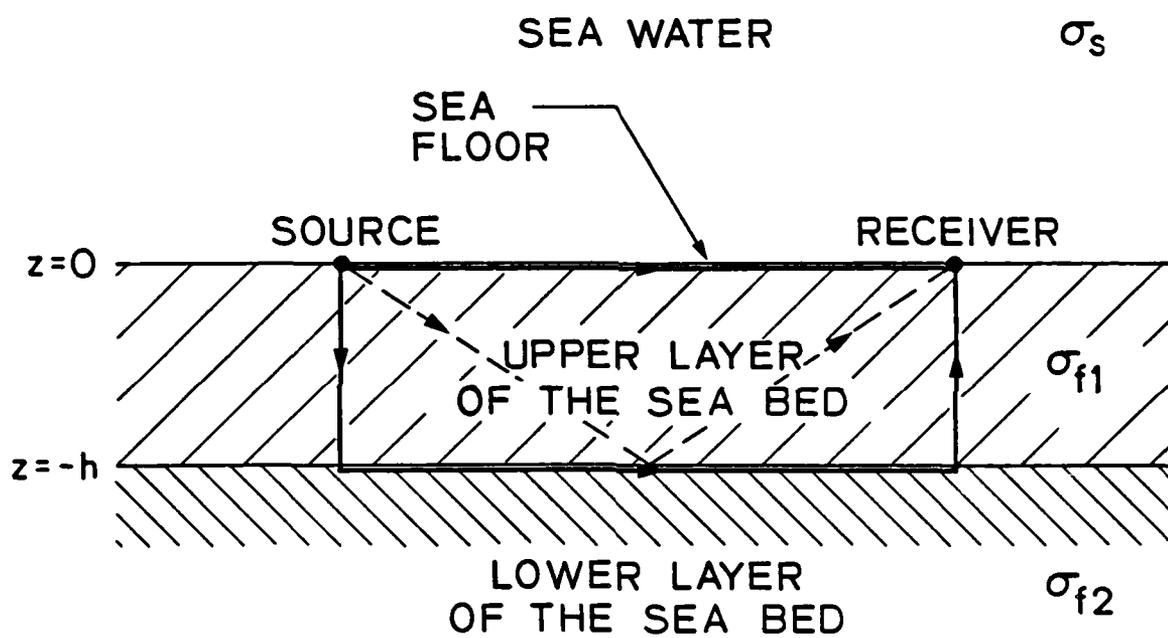
Figure 5.1. Geometry for a sea bed containing two conducting layers..

In practice, it may not be possible to locate the receiver precisely at the interface. Another extension would be to place the receiver some distance above the sea/sea-bed interface and then calculate the fields for this configuration. The integrals for the field expressions will then require an additional exponential term $e^{-u_s z}$ because of the attenuation of the signal as it propagates the vertical distance between the source and receiver in the sea water. As a result of this attenuation, the signals at some vertical distance away from the source will be smaller than on the sea floor.

REFERENCES

Bannister, P. R., "Determination of the electrical conductivity of the sea bed in shallow waters," *Geophysics, 33,* 995–1003, 1968a.

Bannister, P. R., "Determination of the electrical conductivity of the sea bed in shallow waters," *Geophysics, 33,* 995–1003, 1968b.

Bannister, P. R., and R. L. Dube, Numerical results for modified image theory quasi-static range subsurface-to-subsurface and subsurface-to-air propagation equations, Tech. Rep. 5775, 30 pp., Naval Underwater Systems Center, New London, Connecticut, 1977.

Banos, A., *Dipole Radiation in the Presence of a Conducting Half Space,* 245 pp., Pergamon Press, New York, 1966.

Brock-Nannestad, L., "Determination of the electrical conductivity of the seabed in shallow waters with varying conductivity profile," *Electron. Letters, 1,* 274–276, 1965.

Bubenik, D. M., "A practical method for the numerical evaluation of Sommerfeld Integrals," *IEEE Trans. Ant. Prop., AP-25,* 904–906, 1977.

Bubenik, D. M., and A. C. Fraser-Smith, "ULF/ELF electromagnetic fields generated in a sea of finite depth by a submerged vertically-directed harmonic magnetic dipole," *Radio Sci., 13,* 1011–1020, 1978.

Burrows, C. R., "Radio communication within the earth's crust," *IEEE Trans. Ant. Prop., AP-11,* 311–317, 1963.

Butterworth, S., "The distribution of the magnetic field and return current round a submarine cable carrying alternating current.-Part 2," *Phil. Trans. Roy. Soc. London, Ser. A, 224,* 141–184, 1924.

Computation Laboratory of Harvard University, *Tables of the Generalized Exponential-Integral Functions,* 416 pp., Harvard Univ. Press, Cambridge, Mass., 1949.

Coggon, J. H., and H. F. Morrison, "Electromagnetic investigation of the sea floor," *Geophysics, 35,* 476–489, 1970.

Drysdale, C. V., "The distribution of the magnetic field and return current round a submarine cable carrying alternating current.-Part 1," *Phil. Trans. Roy. Soc. London, Ser. A, 224,* 95–140, 1924.

Fraser-Smith, A. C., and D. M. Bubenik, "ULF/ELF electromagnetic fields generated at the sea surface by submerged magnetic dipoles," *Radio Sci., 11,* 901–913, 1976.

Fraser-Smith, A. C., and D. M. Bubenik, "ULF/ELF electromagnetic fields generated above a sea of finite depth by a submerged vertically-directed harmonic magnetic dipole," *Radio Sci., 14,* 59–74, 1979.

Hansen, R. C., "Radiation and reception with buried and submerged antennas," *IEEE Trans. Ant. Prop., AP-11,* 207–216, 1963.

Hermance, J. F., and W. R. Peltier, "Magnetotelluric fields of a line current," *J. Geophys. Res., 75,* 3351–3356, 1970.

Inan, A. S., A. C. Fraser-Smith, and O. G. Villard, Jr., ULF/ELF electromagnetic fields produced in sea water by linear current sources, Tech. Rep. E721-1, 104 pp., Stanford Electronics Laboratories, Stanford University, California, 1982.

Inan, A. S., A. C. Fraser-Smith, and O. G. Villard, Jr., "ULF/ELF electromagnetic fields produced in a conducting medium of infinite extent by linear current sources of infinite length," *Radio Sci.*, *18*, 1383–1392, 1983.

King, R. W. P., and G. S. Smith, *Antennas in Matter*, Sect. 11.12, MIT Press, 1981.

Kraichman, M. B., *Handbook of Electromagnetic Propagation in Conducting Media*, Second Printing, U.S. Government Printing Office, Washington, D.C., 1976.

Liebermann, L. N., "Other electromagnetic radiation," in *The Sea*, Ed. M. N. Hill, Volume 1, Physical Oceanography, Chap. 11, John Wiley and Sons, New York, 1962.

Lowell, H. H., Tables of the bessel-kelvin functions ber, bei, ker, kei, and their derivatives for the argument range 0(0.01)107.50, Tech. Rep. R-32, NASA, Lewis Res. Center, Cleveland, Ohio, 1959.

Moore, R. K., The theory of radio communication between submerged submarines, Ph. D. Thesis, Cornell University, 1951.

Moore, R. K., and W. E. Blair, "Dipole radiation in a conducting half-space," *J. Res. Nat. Bur. Stand. Sect. D*, *65D*, 547–563, 1961.

Moore, R. K., "Radio communication in the sea," *IEEE Spectrum*, *4*, 42–51, 1967.

Mott, H., and A. W. Biggs, "Very-Low-Frequency Propagation below the bottom of the sea," *IEEE Trans. Ant. Prop.*, *AP-11*, 323–329, 1963.

Pickard, G. L., and W. J. Emery, *Descriptive Physical Oceanography, An Introduction*, Fourth Enlarged Edition, 249 pp., Pergamon Press, New York, 1982.

Ramaswamy, V., H. S. Dosso, and J. T. Weaver, "Horizontal magnetic dipole embedded in a two-layer conducting medium," *Can. J. Phys.*, *50*, 607–616, 1972.

Soderberg, E. F., "ELF noise in the sea at depths from 30 to 300 meters," *J. Geophys. Res.*, *74*, 2376–2387, 1969.

Sunde, E. D., *Earth Conduction Effects in Transmission Systems*, 370 pp., Dover Publications, New York, 1968.

Tranter, C. J., *Integral Transforms in Mathematical Physics*, pp. 67–72, Methuen, London, 1956.

Wait, J. R., "Electromagnetic fields of current-carrying wires in a conducting medium," *Can. J. Phys.*, *30*, 512–523, 1952a.

Wait, J. R., "Current-carrying wire loops in a simple inhomogeneous region," *J. Appl. Phys.*, *23*, 497–498, 1952b.

Wait, J. R., "The fields of a line source of current over a stratified conductor," *Appl. Sci. Res., Sec. B*, *3*, 279–292, 1953.

Wait, J. R., and L. L. Campbell, "The fields of an oscillating magnetic dipole immersed in a semi-infinite conducting medium," *J. Geophys. Res.*, *58*, 167–178, 1953.

Wait, J. R., "The electromagnetic fields of a horizontal dipole in the presence of a conducting half-space," *Can. J. Phys., 39*, 1017–1028, 1961.

Wait. J. R., *Electromagnetic Waves in Stratified Media*, Chap. 2, Pergamon Press, New York, 1962.

Wait, J. R., and K. P. Spies, "Subsurface electromagnetic fields of a line source on a conducting half-space," *Radio Sci., 6*, 781–786, 1971.

Wait, J. R., "Project Sanguine," *Science, 178*, 272–275, 1972.

Wait, J. R., and K. P. Spies, "Electromagnetic propagation in an idealized earth crust waveguide, Part I," *Pure Appl. Geophys., 101*, 174–187, 1972a.

Wait, J. R., and K. P. Spies, "Electromagnetic propagation in an idealized earth crust waveguide, Part II," *Pure Appl. Geophys., 101* 188–193, 1972b.

Wait, J. R., and K. P. Spies, "Dipole excitation of ultra-low-frequency electromagnetic waves in the earth crust waveguide," *J. Geophys. Res., 77*, 7118–7120, 1972c.

Wait, J. R., and K. P. Spies, "Subsurface electromagnetic fields of a line source on a two-layer earth," *Radio Sci., 8*, 805–810, 1973.

Weaver, J. T., "The quasi-static field of an electric dipole embedded in a two-layer conducting half-space," *Can. J. Phys., 45*, 1981–2002, 1967.

Wheeler, H. A., "Radio-wave propagation in the earth's crust," *J. Res. Nat. Bur. Stand. Sect. D, 65*, 189–191, 1960.

Wright, C., "Leader Gear," pp. 177–184 in *Proc. Symposium on Underwater Electromagnetic Phenomena*, Ed. G. W. Wood, 216 pp., 1953.

Young, A., and A. Kirk, Bessel Functions, Part IV; Kelvin Functions, in *Royal Soc. Math. Tables, 10*, 97 pp., Cambridge Univ. Press, 1964.

Young, P. D., and C. S. Cox, "Electromagnetic active source sounding near the East Pacific Rise," *Geophys. Res. Letters, 8*, 1043–1046, 1981.

DISTRIBUTION LIST

Organization	No. of Copies	Organization	No. of Copies
Director		Naval Research Laboratory	
Defense Advanced Research		Information Technology Division	
Projects Agency		ATTN: J.R. Davis	1
ATTN: Project Management	2	4555 Overlook Avenue, SW	
GSD, R. Alewine	1	Washington, D.C. 20375	
STO, D.D. Lewis	1		
1400 Wilson Blvd		Naval Ocean Systems Center	
Arlington, VA 22209		ATTN: Library	1
		K.L. Grauer	1
Defense Technical		C.F. Ramstedt	1
Information Center	12	Y. Richter	1
Cameron Station		271 Catalina Boulevard	
Alexandria, VA 22314		San Diego, CA 95152	
Office of Naval Research		Naval Electronic Systems	
ATTN: Code 222	1	Command	
Code 414	1	ATTN: PME-110-112	1
Code 420	1	PME-110-X1	1
Code 425	1	Department of the Navy	
800 North Quincy Street		Washington, D.C. 20360	
Arlington, VA 22217			
		Naval Underwater Systems Center	
Office of Naval Research		New London Laboratory	
Resident Representative	1	ATTN: P. Bannister	1
University of California,		A. Bruno	1
San Diego		J. Orr	1
La Jolla, CA 92093		E. Soderberg	1
		New London, CT 06320	
Office of Naval Research			
Resident Representative	1	Naval Surface Weapons Center	
Stanford University		White Oak Laboratory	
Durand Building, Room 165		ATTN: J.J. Holmes	1
Stanford, CA 94305		P. Wessel	1
		Silver Spring, MD 20910	
Assistant Deputy Undersecretary			
of Defense (C^3)		David W. Taylor Naval Ship	
ATTN: T.P. Quinn	1	Research & Development Center	
Pentagon		ATTN: W. Andahazy	1
Washington, D.C. 20301		P. Field	1
		Annapolis, MD 21402	

Organization	No. of Copies	Organization	No. of Copies
Office of the Assistant Secretary of the Navy (R, E&S) ATTN: J. Hull Washington, D.C. 20350	1	Naval Air Development Center ATTN: J. Shannon Warminster, PA 18974	1
Naval Ocean R & D Activity ATTN: D.L. Durham	1	Naval Ocean Systems Center ATTN: R. Buntzen	1
D.W. Handschumacher	1	C. Fuzak	1
K. Smits NSTL Station Bay St. Louis, MS 39522	1	P. Hansen 271 Catalina Boulevard San Diego, CA 95152	1
Naval Oceanographic Office ATTN: O.E. Avery	1	Director Defense Nuclear Agency ATTN: RAAE	1
T. Davis	1	DDST	1
G.R. Lorentzen NSTL Station Bay St. Louis, MS 39522	1	RAEV Washington, D.C. 20305	1
Naval Air Systems Command ATTN: B.L. Dillon Washington, D.C. 20361	1	SRI International ATTN: D.M. Bubenik	1
		J.B. Chown	1
		J.G. Depp	1
		R.C. Honey	1
Naval Intelligence Support Center ATTN: G.D. Batts	1	W.E. Jaye 333 Ravenswood Avenue	1
W. Reese	1	Menlo Park, CA 94025	
4301 Suitland Road Washington, D.C. 20390		R. & D. Associates ATTN: C. Greifinger P.O. Box 9695 Marina del Rey, CA 90291	1
Naval Postgraduate School Department of Physics and Chemistry ATTN: O. Heinz Monterey, CA 93940	1	Pacific-Sierra Research Corp. ATTN: E.C. Field, Jr. 12340 Santa Monica Blvd Los Angeles, CA 90025	1
Naval Coastal Systems Center ATTN: R.H. Clark M.J. Wynn Panama City, FL 32407	1	TASC ATTN: J. Czika, Jr. 1700 N. Moore Street, Suite 1220 Arlington, VA 22209	1

DISTRIBUTION LIST (Continued)

Organization	No. of Copies	Organization	No. of Copies
Naval Weapons Center ATTN: R.J. Dinger China Lake, CA 93555	1	University of California Scripps Institute of Oceanography ATTN: C.S. Cox La Jolla, CA 92093	1
Johns Hopkins University Applied Physics Laboratory ATTN: L.W. Hart 　　　　H. Ko Johns Hopkins Road Laurel, MD 20810	1 1	Lockheed Palo Alto Research 　Laboratory ATTN: J.B. Cladis 　　　　W.L. Imhof 　　　　J.B. Reagan 　　　　M. Walt 3251 Hanover Street, Bldg 255 Palo Alto, CA 94304	1 1 1 1
La Jolla Institute ATTN: K. Watson La Jolla, CA 92407	1		
E.G. & G. ATTN: L.E. Pitts P.O. Box 398 Riverdale, MD 20840	1	Chief Air Force Technical 　Applications Center HQUSAF Patrick AFB, FL 32925	1
University of Texas, Austin Geomagnetics and Electrical 　Geoscience Laboratory ATTN: F.X. Bostick, Jr. Austin, TX 78712	1	Commander Air Force Systems Command Andrews AFB, MD 20331	2
Commander Rome Air Development 　Center/EEPS ATTN: P.A. Kossey Hanscom AFB, MA 01731	1	Commander Air Force Geophysics Laboratory ATTN: Technical Library Hanscom AFB, MA 01731	1

END

FILMED

2-85

DTIC